BABEȘ-BOLYAI UNIVERSITY
FACULTY OF PHYSICS
PHYSICS DOCTORAL SCHOOL

Applications of composites based on TiO_2-WO_3 and noble metals (Au) for SERS detection and photocatalytic degradation of chemical pollutants

Ph.D. Thesis

Scientific advisor:

Prof. Dr. habil. Monica Baia

Ph.D. Student:

István-Attila Székely

Cluj-Napoca

2023

Table of Contents

Keywords:

Titanium dioxide; tungsten trioxide; gold nanoparticles; heterostructures; hydrothermal synthesis; heterogenous photocatalysis; photocatalysts; sensor; SERS

1. Introduction

Environmental pollution is a severe worldwide problem that can lead to serious health issues and diseases [1,2]. Water, air, and soil pollution are the most significant contributors to the declining health of an individual [2,3] and can be classified into primary or secondary pollution classes. The former is considered the pollution from industry (Figure 1) since it is the leading water polluter, releasing millions of tons of harmful chemicals like reactants [4], solvents [5], lubricants [6], oils [7], and dyes [8] into the environment [9]. Secondary pollution can be considered the one produced in households, hospitals, and agriculture (Figure 1), such as alkaloids [10], pharmaceuticals and their by-products [11], disinfectants and their by-products [12], microplastics [13], pesticides and fertilizers [14,15]. Some pollutants are present in polluted water in small concentrations (micromolar and nanomolar) [16,17], and for efficient removal of the pollutants, the ability to detect them is just as important as removing them.

Figure 1. Primary (industries, transportation, and electronics) and secondary (households, hospitals, and agriculture) sources of environmental pollution.

The detection of organic pollutants can be carried out qualitatively or quantitively [18,19]. Qualitative detection of organic pollutants can be considered a viable option because it is cost-effective, straightforward to use, provides a fast response, and is observable with the naked eye (e.g., color change [20]). The sensors' ability to detect pollutants is due to their photochromic (PC) and electrochromic (EC) properties [21]. The drawback of qualitative sensors is their modest limit of detection (LOD). Quantitative detection of organic pollutants is a more exact method, and it can detect chemicals in very low concentrations (10^{-5} – 10^{-10} M). For this purpose, techniques such as

HPLC, GC, GC-MS, and SERS can be employed [22–26]. The highly sensitive SERS technique is widely utilized to detect chemical compounds even in ultralow concentrations (10^{-12} – 10^{-14} M) [27–29].

Many well-known methods are used for water treatment, such as biological (liquefaction, biodegradation, and phytoremediation), chemical (ion exchange, ozonation, and electrochemistry), or physical approaches (precipitation, flotation, and adsorption) [30–33], but these methods either have a low efficiency or are expensive. A relatively new technology, specifically the advanced oxidation processes (AOPs), can serve as a viable option for water treatment since it is cost-effective, environmentally friendly, easily applicable, and, most importantly, highly efficient in removing organic pollutants [34]. Methods such as Fenton oxidation, photolysis, ozonation, or heterogenous photocatalysis are considered among the AOPs [35]. From them, heterogenous photocatalysis is the most widely applied approach in research [36] since, after the photocatalytic process the spent photocatalysts can be recovered and utilized after several cycles [37,38], although in some cases, the photocatalysts need to be regenerated [39,40].

Aim of the Ph.D. thesis

The aim of this thesis was focused on the synthesis of heterostructures (based on TiO_2/WO_3 and $Au/TiO_2/WO_3$) that can efficiently remove several model pollutants (MPT) under UV and Vis irradiation and can be employed as sensors to detect chemical contaminants. This research also investigated the possible links between the heterostructures' structural and optical properties and their photocatalytic and sensorial activity.

Structure of the thesis

I. Impact of different hydrohalic acids, sodium and potassium salts and their electronegativity on tungsten oxide semiconductors' morpho-structural properties; and on TiO_2/WO_3, $TiO_2/WO_3 \cdot 0.33H_2O$ heterojunctions photocatalytic performance
   - Hydrothermal crystallization of tungsten oxides utilizing $Na_2WO_4 \cdot 2H_2O$, sodium salts (NaF, NaCl, NaBr, NaI) or potassium salts (KF, KCl, KBr, KI), and 3 M HCl solution
   - Hydrothermal crystallization and annealing of tungsten oxides semiconductors utilizing $(NH_4)_6H_2W_{12}O_{40} \cdot xH_2O$, and hydrohalic acids (HF, HCl, HBr, HI)
   - Photocatalytic efficiency investigations of TiO_2/WO_3 composites under UV light exposure: methyl orange (MO) photocatalytic decolorization
   - Influence of electronegativity on tungsten oxides' surface chemistry, structural, optical properties, and the assessed photocatalytic performance

II. Optimization of TiO_2 to WO_3 ratio in TiO_2/WO_3 heterostructures for enhanced photocatalytic efficiency under UV light exposure
   - Preparation of TiO_2/WO_3-AMT-HCl heterostructures with various TiO_2 and WO_3 ratios
   - Optical and structural characterization of the TiO_2/WO_3-AMT-HCl heterostructures
   - Photocatalytic efficiency assessment of the TiO_2/WO_3-AMT-HCl heterostructures under UV light exposure: oxalic acid (OA) photocatalytic degradation
   - Qualitative detection of OA solutions under UV-A exposure with TiO_2/WO_3-AMT-HCl heterostructures (76:24 TiO_2 to WO_3 ratio)

III. Optimization of TiO_2/WO_3 heterostructures *via* pH adjustment of the TiO_2-WO_3-AMT-HCl-WO_3-HW ternary composites for enhanced photocatalytic efficiency
   - Preparation of the TiO_2-WO_3-AMT-HCl-WO_3-HW composites
   - Morpho-structural and optical characterization of the TiO_2-WO_3-AMT-HCl-WO_3-HW composites
   - Photocatalytic efficiency assessment of the TiO_2-WO_3-AMT-HCl-WO_3-HW composites under UV light exposure: OA, MO, and phenol (PHE) photocatalytic degradation

- Correlations established between the pH-adjusted ternary composites' structural and optical parameters and their photocatalytic efficiencies

IV. Electron trapping in TiO_2/WO_3-NWH-NaCl, TiO_2-WO_3-AMT-HCl heterostructures for applications in AOPs and sensing

- Preparation of the TiO_2/WO_3-NWH-NaCl, and TiO_2/WO_3-AMT-HCl heterostructures
- Structural and optical characterization of commercial TiO_2, WO_3-NWH-NaCl, and WO_3-AMT-HCl metal oxides
- Charge transfer in TiO_2/WO_3-NWH-NaCl heterostructures (EtOH vapor detection under brief UV light irradiation)
- The photocatalytic performance of TiO_2/WO_3-NWH-NaCl, and TiO_2/WO_3-AMT-HCl heterostructures under UV light exposure (OA and MO photodegradation)
- TiO_2/WO_3 heterostructures sensory applicability in open systems (OA detection under direct sunlight)

V. Applications in heterogeneous photocatalysis and surface-enhanced Raman spectroscopy of WO_3 and $WO_3 \cdot 0.33H_2O$ morphology-dependent $Au/TiO_2/WO_3$ heterojunctions

- Synthesis of the $Au/TiO_2/WO_3$ heterojunctions
- Morpho-structural and optical characterization of the $Au/TiO_2/WO_3$ heterojunctions
- Photocatalytic recyclability and stability of the $Au/TiO_2/WO_3$ heterojunctions
- Crystal violet dye detection on $Au/TiO_2/WO_3$ substrates using SERS
- Stability of the $Au/TiO_2/WO_3$ composite as SERS substrates

Hydrothermal crystallization of electronegativity-dependent WO_3 and $WO_3 \cdot 0.33H_2O$ semiconductors

Three sample series were obtained employing the hydrothermal crystallization method. In the case of the first and second series, the precursor was the sodium tungstate dihydrate (NWH, 99.9%, Sigma–Aldrich), and ammonium metatungstate hydrate (AMT, 99.9%, Sigma–Aldrich) was the precursor for the third series. The shaping agents of the first and second series were sodium (NaF, NaCl, NaBr, NaI) and potassium salts (KF, KCl, KBr, KI), whereas concentrated hydrohalic acids (HF, HCl, HBr, HI) were the shaping agents in the case of the third series. Concerning the

first and second series, the NWH precursor and the corresponding sodium or potassium salts were added into distilled water to obtain the desired solution, then the solutions' pH was adjusted to a pH value of ≈ 2. The protonated solutions were stirred, then transferred to an autoclave for the hydrothermal treatment that occurred at 180 °C for 24 hours. The synthesized tungsten oxides further on will be referred to as WO_3-NWH-NaX in the case of the first series and as WO_3-NWH-KX in the case of the second series.

Regarding the third series, the AMT precursor and the corresponding hydrohalic acids were added into distilled water, then they were stirred. After transferring the solutions into the autoclave, the hydrothermal crystallization was carried out for 4 hours at 180 °C. The obtained materials were also annealed in a furnace for 30 minutes at 500 °C. The synthesized tungsten oxides further on will be referred to as WO_3-AMT-HX. Figure 2 summarizes the 11 obtained tungsten oxide semiconductors.

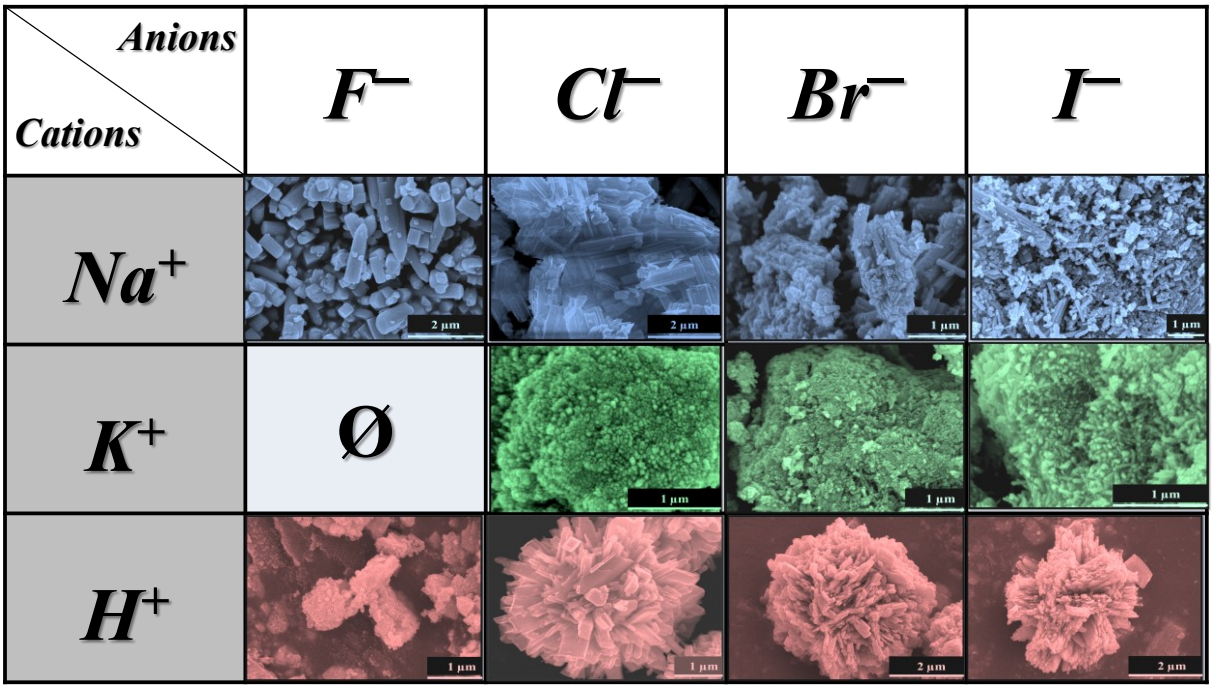

Figure 2. SEM micrographs of the electronegativity-dependent tungsten oxides.

The obtained tungsten oxide semiconductors exhibited no photocatalytic activity, regardless of the chosen model pollutant: oxalic acid (OA), phenol (PHE) or methyl orange (MO) nor under UV or Vis light exposure. TiO_2/WO_3 composites were prepared *via* mechanical mixing

to overcome the WO_3 semiconductors' idleness, where commercial Evonik Aeroxide TiO_2 (P25) was selected as a counterpart for the tungsten oxides due to its wide availability, cost-effectiveness and high photocatalytic efficiency under UV light exposure for a wide variety of pollutants. Regarding the decolorization of MO under UV light exposure, the best-performing composite from the first series was TiO_2/WO_3-NWH-NaI, from the second series was TiO_2/WO_3-NWH-KI, and from the third series, the best-performing composites were TiO_2/WO_3-AMT-HCl and TiO_2/WO_3-AMT-HF, as they reached MO decolorization rates of 67.4%; 69.3%; 84.6% and 87.7%. Commercial TiO_2 reached an 82.8% MO decolorization rate. From the obtained 11 tungsten oxide semiconductors and 11 TiO_2/WO_3 composites, WO_3-NWH-NaCl and WO_3-AMT-HCl tungsten oxides, and TiO_2/WO_3-NWH-NaCl and TiO_2/WO_3-AMT-HCl composites were selected to be studied in greater detail due to their advantageous surface chemistry, structural and optical properties, and furthermore because their ample synthesis yield (WO_3 semiconductors').

Optimization of the TiO_2/WO_3 heterostructures to obtain composites with enhanced photocatalytic efficiencies and sensing properties under UV light exposure

The first optimization stage involved determining the optimal TiO_2 and WO_3 percentages in the TiO_2/WO_3 heterostructures and their preparation *via* mechanical mixing. The optimal TiO_2 to WO_3 ratio was determined through photocatalytic removal of 3 mM OA under UV light exposure with various TiO_2/WO_3 composites. The best-performing TiO_2/WO_3 heterostructure removed 99% of the OA pollutant, and in consequence, it was selected to detect and remove OA in different concentrations simultaneously. Five TiO_2/WO_3 heterostructures with various TiO_2 and WO_3 percentages were prepared.

For the second optimization stage, novel TiO_2/WO_3 heterostructures were prepared by incorporating two types of WO_3 with diverse geometries and different structural and optical properties. The novel TiO_2/WO_3 heterostructures were obtained *via* the pH adjustment method: commercial TiO_2, WO_3-HW, and WO_3-AMT-HCl semiconductors were added to distilled water to obtain the suspensions, then the suspensions' pH was adjusted to pH values of 1, or 4, or 7, or 10. The photocatalytic efficiencies of the obtained ternary composites were assessed by removing

model pollutants such as OA, MO, or PHE under UV light exposure. The best-performing ternary composites efficiently removed 72.3% and 95.9% of OA (TiO_2 removed 47.9%); 83.5% and 87.7% of PHE (TiO_2 removed 86.8%); and 97.0% and 98.7% of MO (TiO_2 removed 82.8%). Four novel TiO_2/WO_3 heterostructures were prepared.

The third optimization stage involved preparing the TiO_2/WO_3 composites through the simple suspension method. To obtain the suspensions, commercial TiO_2, WO_3-NWH-NaCl, or WO_3-AMT-HCl were added to distilled water. The photocatalytic efficiencies of the obtained TiO_2/WO_3 heterostructures were investigated under UV light exposure by removing OA and MO model pollutants. The best-performing composites removed efficiently 77.2% of OA (TiO_2 removed 95.7%), 88.9%, and 96.7% of MO (TiO_2 removed 82.8%). The obtained TiO_2/WO_3 heterostructures sensing capabilities under UV light or direct sunlight exposure were also assessed in closed and open systems. Two TiO_2/WO_3 heterostructures were prepared.

Synthesis of tungsten oxide morphology-dependent $Au/TiO_2/WO_3$ heterojunctions with applications in heterogeneous photocatalysis and surface-enhanced Raman spectroscopy

Tungsten oxides (WO_3-HW, WO_3-NWH, WO_3-AMT) with three different geometries (blade-like, rod-like, and flower-like), commercial TiO_2, and $HAuCl_4$ solutions were employed to synthesize the $Au/TiO_2/WO_3$ heterojunctions. A slightly modified Turkevich-Frens method was utilized to deposit the gold nanoparticles (Au NPs) on the TiO_2/WO_3 composites' surface. Two deposition routes were utilized for the reduction of Au NPs: the heat-assisted route (HA) and the time-assisted route (TA). The obtained $Au/TiO_2/WO_3$ heterojunctions' photocatalytic efficiency was assessed by removing model pollutants such as OA, PHE, and MO under UV light, respectively aspirin (ASP) under Vis light exposure. The $Au/TiO_2/WO_3$ heterojunctions were employed as SERS substrates for detecting crystal violet dye in 10^{-6} – 10^{-8} M concentration range. The best-performing heterojunctions removed efficiently 96.6% of OA; 99.0% of PHE; 97.9% of MO; and 82.1% of ASP; moreover, the best-performing substrates reached a 10^{-8} M detection limit for the crystal violet dye. Six $Au/TiO_2/WO_3$ heterojunctions were prepared.

2. Morphological and structural characterization of the materials

2.1 Scanning Electron Microscopy (SEM)

Scanning Electron Microscopy (SEM) micrographs were acquired using a Hitachi S-4700 Type II cold field emission scanning electron microscope equipped with a Röntec QX2-EDS spectrometer. The apparatus was operated at an accelerating voltage of 30 kV.

2.2 Energy Dispersive Spectroscopy (EDX)

EDX analysis was performed with a Hitachi S-4700 Type II microscope (Japan, Tokyo) equipped with a cold field emission gun using a Röntec XFlash Detector 3001 detector (Bruker, Karlsruhe, Germany).

2.3 Transmission Electron Microscopy (TEM)

In order to investigate the nano-scale assembly of the $Au/TiO_2/WO_3$ heterostructures, transmission electron microscopy (TEM) analyses were conducted using an FEI Tecnai F20 field emission high-resolution transmission electron microscope. The microscope was operated at an accelerating voltage of 200 kV and was equipped with an Eagle 4k CCD camera. The samples were dispersed in distilled water and applied onto carbon-coated Formwar-Cu grids using a drop-casting technique. The size distribution of the gold nanospheres was ascertained *via* analysis of transmission electron microscopy (TEM) images, wherein no less than 100 nanoparticles were accounted for in each case.

2.4 X-ray Powder Diffraction (XRD)

XRD diffractograms were recorded on a Shimadzu 6000 diffractometer (Shimadzu Corporation, Kyoto, Japan) using a Cu-K_α source ($\lambda = 1.5406$ Å). Metal oxides' crystalline phases were identified using the JCPDS database. The majority of XRD patterns were acquired between 20° – 40°, in some cases between 20° – 50°.

The speed, in all cases, was $2°\cdot min^{-1}$. The average crystallite size of the tungsten oxides was determined according to the Debye Scherrer equation (Equation 1) [41].

$$D = (K \cdot \lambda) \cdot (\cos\theta \cdot \beta)^{-1} \quad (1)$$

where D is the crystallite size of the nanoparticle (nm), the Scherrer constant is K (0.89), λ is the wavelength of the employed X-ray beam (0.15405 nm), θ is the Bragg angle, and β is the full width at half maximum (FWHM) of the diffraction peak.

2.5 Diffuse Reflectance Spectroscopy (DRS)

Reflectance spectra were recorded on a JASCO-V650 spectrophotometer (Easton, Maryland, United States) fitted with an ILV-724 integration sphere (Easton, Maryland, United States). Diffuse reflectance spectra of each material were acquired in the 250 – 800 nm spectral domain. $BaSO_4$ was the reference material. In most cases, the band gap (E_g) values were estimated from the diffuse reflectance spectra by employing the Kubelka-Munk equation (2) or the Tauc plot, respectively the David-Mott relation (3) [42–44].

$$f(R_\infty) = \frac{(1-R_\infty)^2}{2R_\infty} = \frac{K}{S} \quad (2)$$

$$(\alpha h\nu)^n = K(h\nu - E_g) \quad (3)$$

The E_g values of the pH-adjusted TiO_2-WO_3-AMT-HCl-WO_3-HW composites were rather difficult to calculate with the Kubelka-Munk or Tauc plot approach due to the three metal oxides present in the composites. So, to overcome the issue of the E_g values, they were estimated by employing the first-order derivative of the composite's reflectance spectra, then a second order polynomial Savitzky – Golay smoothing with a 10-point window was applied. Utilizing the peak assignment tool, respectively, the Menke relation [45], the E_g values of the three components were determined in each composite system.

2.6 Fourier Transform Infrared Spectroscopy (FT-IR spectroscopy)

The samples FT-IR absorption spectra were acquired by employing a Jasco 6000 (Tokyo, Japan) spectrometer in reflection configuration at 22 – 23 °C. The absorption spectra were recorded

in the range between 400 and 4000 cm^{-1}. The resolution of the absorption spectra was 4 cm^{-1}. Using KBr, all investigated materials were prepared as pellets in a hydraulic press.

2.7 Raman Spectroscopy

Raman spectra of the samples were recorded with a multilaser confocal Renishaw inVia Reflex Raman spectrometer equipped with a RenCam CCD detector. The 532 nm laser was applied as an excitation source. The Raman spectra were collected using a 0.9NA objective of 100 × magnification. The integration time was 30 s, 1800 lines/mm grating for all spectra, and 10% of the maximum laser intensity – laser power of 20 mW. The spectral resolution was 4 cm^{-1}.

Several Raman bands ratios were estimated to approximate surface defects. Regarding pH-adjusted composites, the ratios of I_{324} cm^{-1}/I_{714} cm^{-1} and I_{943} cm^{-1}/I_{805} cm^{-1} WO_3 metal oxides were analyzed; concerning the electronegativity-dependent tungsten oxides the ratio of I_{327}/I_{701} (sodium halide series – NaX), I_{327}/I_{804} (potassium halide series – KX), and I_{327}/I_{802} (hydrohalic acids series – HX). Regarding $Au/TiO_2/WO_3$ composites the TiO_2-A and hydrated WO_3 Raman band ratios were calculated (I_{515}/I_{396} and I_{810}/I_{926}) to estimate the influence of surface modifications.

2.7.1 Surface Enhanced Raman Spectroscopy (SERS)

SERS spectra of the CV dye were recorded using a λ = 633 nm laser and a microscope objective with a NA of 0.35 at 20× magnification, in the range of 100–1800 cm^{-1}. The integration time was 90 s for all spectra with a laser power of 17 mW. The Raman and SERS spectra had a spectral resolution of 4 cm^{-1}. To demonstrate the substrates' SERS stability, CV spectra were recorded at various concentrations (10^{-6}–10^{-8} M) after ≈ 4 years under similar conditions.

2.8 X-ray Photoelectron Spectroscopy (XPS)

XPS measurements were conducted using a SPECS Phoibos 150 MCD system equipped with an Al-K_α source (1486.6 eV) at 14 kV and 20 mA, a hemispherical analyzer, and a charge neutralization device. All samples were fixed on a double-sided carbon tape that was completely

covered by them. The binding energy scale was charged, referenced to the C 1s at 284.6 eV. High-resolution W 4f and O 1s, respectively W 4f, W 4d, W 4p, Ti2p, and Au 4f spectra were obtained using an analyzer to pass energy of 20 eV in steps of 0.05 eV for the analyzed samples. The data analysis was carried out with CasaXPS software.

2.9 Photoluminescence Spectroscopy (PL spectroscopy)

The PL spectra were measured using a fluorescence spectrophotometer, specifically the Jasco LP-6500 spectrofluorometer manufactured by Jasco in Vienna, Austria. The spectrophotometer had a spectral resolution of 1 nm and utilized a Xenon lamp as the excitation source. Additionally, it was equipped with an epifluorescence accessory in the form of the EFA 383 module. The measurements were recorded within the 350–800 nm wavelength range, using fixed excitation wavelengths at 365 and 450 nm.

3. Photocatalytic setups and experiments

To perform the photocatalytic tests, double-walled Pyrex glass tubes (Pyrex photoreactors) were utilized (V = 140 mL), which could warrant a constant temperature of 25 °C through a thermostat. The duration of the photocatalytic tests under UV-A irradiation was 2 hours, and under Vis irradiation was 4 hours. The photocatalytic efficiency of TiO_2, TiO_2/WO_3 and $Au/TiO_2/WO_3$ heterostructures, respectively, was determined by employing Equation 4.

$$X = \left[1 - \left(\frac{C_{tf}}{C_0}\right)\right] \times 100 \quad (4)$$

where X represents the removal rate, C_0 is the original pollutant concentration, C_{tf} represents the pollutant concentration after two hours of UV light irradiation, or after four hours of Vis irradiation.

3.1 Photocatalytic tests performed under UV light irradiation

Photocatalytic assessments were performed with the help of 6 × 6W power fluorescent ultraviolet tubes (λ_{max} = 365 nm), which had been positioned circularly around the Pyrex photoreactor. For all photocatalytic tests under UV-A irradiation, the same parameters were

applied: constant temperature of 25 °C, constant stirring at 500 rpm, constant airflow of 50 – 60 $L \cdot h^{-1}$ (to ensure the continuous flow of dissolved oxygen concentration), and 1 $g \cdot L^{-1}$ catalyst load.

3.2 Photocatalytic tests performed under Vis light irradiation

Photocatalytic assessments were performed with the help of 6 × 6W power fluorescent lamps (VIS, λ_{min} = 400 nm), which were positioned circularly around the Pyrex photoreactor. For all photocatalytic tests under Vis light irradiation, the same parameters were applied: constant temperature of 25 °C, constant stirring at 500 rpm, constant airflow of 50 – 60 $L \cdot h^{-1}$ (to ensure the continuous flow of dissolved oxygen concentration), and 1 $g \cdot L^{-1}$ catalyst load.

3.3 Model pollutants' photocatalytic assessment parameters

For the photodegradation tests performed under UV-A exposure, the chosen contaminants were OA, PHE, and MO. Initial concentration of OA was between 0.05 mM and 5 mM, PHE was 0.5 mM; respectively, for MO was 125 μM. For the photodegradations performed under Vis exposure, ASP was selected as model pollutant. All of the model pollutants solutions were prepared in an aqueous medium.

3.4 Photocatalytic activity assessment by employing High-performance liquid chromatography (HPLC)

Photocatalytic performance of all composites regarding OA and PHE mineralization was evaluated employing Agilent 1100 HPLC. For OA, the following parameters were utilized: the eluent was a 0.06% sulfuric acid aqueous solution, with a 0.8 $mL \cdot min^{-1}$ flow rate; a Grom Resin ZH column utilized as stationary phase, and 206 nm as the detection wavelength. For PHE, the used parameters were: the eluent consisted of a mixture of MeOH and H_2O with a ratio of 1:1.857, the stationary phase used was a BST Nucleosyl C-18 (4 mm × 250 mm) column, and a detection wavelength of 210 nm was utilized.

3.5 Photocatalytic activity assessment by employing UV-Vis spectroscopy

MO concentration can be monitored at 513 nm by means of a JASCO V-650 spectrophotometer (Jasco Inc., Easton, MD, USA) because MO's chemical structure is composed of distinctive functional groups, respectively, aromatic rings that participate in the electronic transitions accountable for the absorption of UV-Vis radiation.

Jasco V650 spectrophotometer was utilized to acquire the UV-Vis spectra of ASP within a wavelength range of 190-400 nm, aiming to monitor its degradation. To determine the pharmaceutical concentration, after each measurement point the recorded spectra was integrated.

4. Results and Discussion

Impact of different hydrohalic acids, sodium and potassium salts and their electronegativity on tungsten oxide semiconductors' morpho-structural properties; and on TiO_2/WO_3, $TiO_2/WO_3 \cdot 0.33H_2O$ heterojunctions photocatalytic performance

T1. Influence of precursors, shaping agents, and the anions electronegativity on the tungsten oxides morpho-structural properties during hydrothermal crystallization.

Utilizing NWH as the WO_3 precursor correspondingly sodium or potassium salts as shaping agents, the morphology of the hydrothermally crystallized tungsten oxides was altered. Sodium salts facilitated bullet or rod-like geometries, while potassium salts led to wire-like geometries that bundled together in a dendritic manner [46]. The crystal structure of the WO_3-NWH-NaX and WO_3-NWH-KX series was similar, as the hexagonal partial hydrate crystalline phase was observed in the XRD patterns of both series (JCPDS file no. 35-1001) [47]. The addition of sodium salts led to structures with higher crystallinity grade, whereas potassium salts led to a lower crystallinity grade (Figure 3), therefore confirming the hypotheses presented in the paragraph discussing the morpho-structural properties of the tungsten oxides, namely that the shaping agents, and correspondingly EN influences the semiconductors' morphology and structure.

Utilizing AMT as the WO_3 precursor, and hydrohalic acids as shaping agents, only when HF was applied as shaping agent the tungsten oxides' geometry was different, as in the other cases a flower-like geometry was observed. The crystalline phase composition was dependent of the applied hydrohalic acids. In the WO_3-AMT-HX series two crystalline phases were identified (Figure 3): monoclinic (MC) WO_3 and hexagonal partial hydrate (HPH). The crystalline phase composition of tungsten oxides can be fine-tuned to obtain materials with solely HPH or MC, respectively, mixed crystalline phases by utilizing AMT as the WO_3 precursor, and hydrohalic acids as shaping agents.

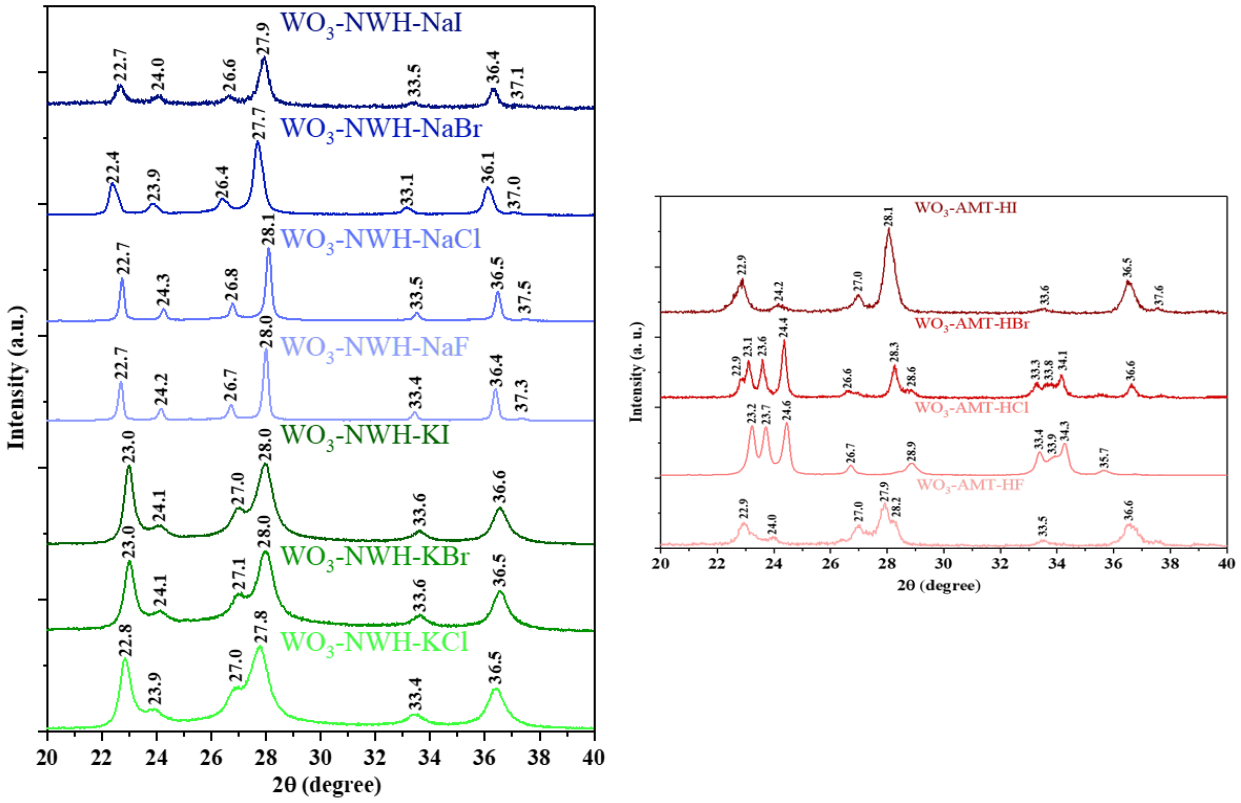

Figure 3. XRD patterns of the electronegativity dependent tungsten oxide semiconductors.

T2. Electronegativity influences differently the TiO_2/WO_3 composites photocatalytic performance when NWH or AMT is employed as precursor.

The photocatalytic performance of the TiO_2/WO_3 composites was evaluated through the photocatalytic removal of MO under UV light exposure (Figure 4). When tungsten oxides from WO_3-NWH-NaX or WO_3-NWH-KX series were used to obtain the mechanically mixed TiO_2/WO_3 composites it was noticed that lower anion electronegativity led to increased MO decolorization rates. However, the composites from neither series proved to be more efficient than the commercial TiO_2. Tungsten oxides from the WO_3-AMT-HX series in composites surpassed the commercial TiO_2's efficiency, and in this case higher anion electronegativity led to increased MO decolorization rates.

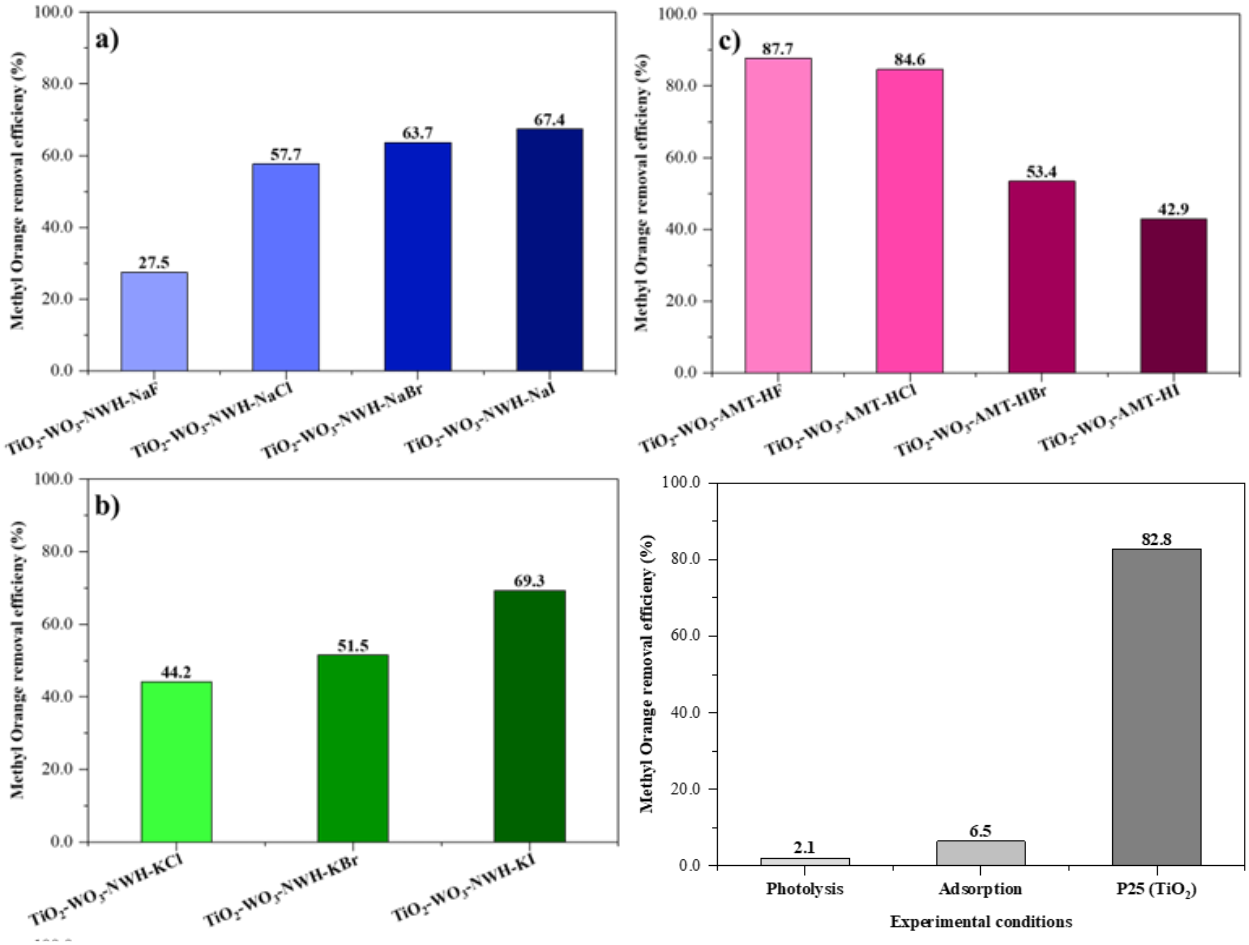

Figure 4. Photocatalytic efficiencies of the TiO_2/WO_3 composites from: a) WO_3-NWH-NaX; b) WO_3-NWH-KX; c) WO_3-AMT-HX series, and of commercial TiO_2.

T3. Influence of electronegativity on tungsten oxides' surface chemistry, optical, structural properties, and on the assessed photocatalytic performance of TiO_2/WO_3 composites.

The influence of the shaping agents' anions electronegativity on the surface chemistry, structural, optical properties and on the TiO_2/WO_3 composites photocatalytic performance was investigated in depth (Figure 5). W^{5+} or W^{6+} species percentage affected the tungsten oxides optical properties. In some cases, W^{5+} species, and in other cases W^{6+} species affected the tungsten oxides optical properties (Figure 5, a and b). In the case of WO_3-AMT-HX series the utilization of hydrohalic acids as shaping agents led to various percentages of W^{5+} species in the tungsten oxides; the W^{5+} proportion directly influenced the tungsten oxides' E_g values (Figure 5, c).

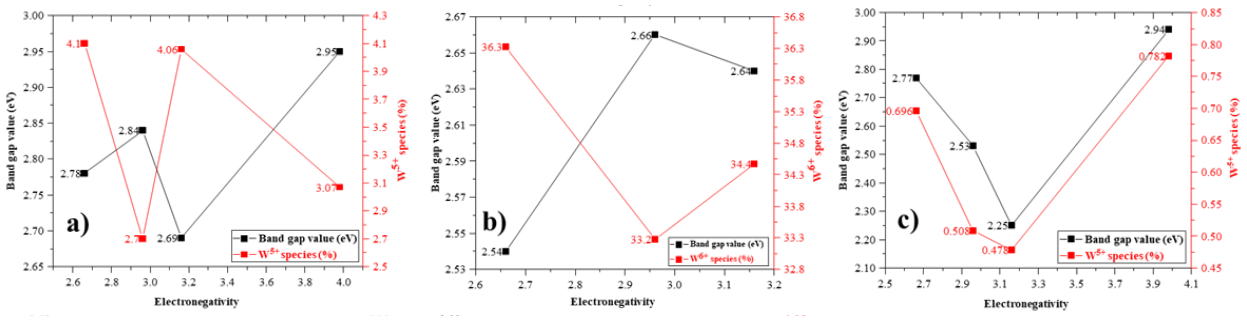

Figure 5. Influence of W^{5+} and W^{6+} species on the WO_3 metal oxides E_g values from: a) WO_3-NWH-NaX; b) WO_3-NWH-KX; c) WO_3-AMT-HX series.

An interesting relationship between MO decolorization rates and surface defects was found, that may seem surprising at first: surface defects abundance inhibited the TiO_2/WO_3 composites' photocatalytic performance (Figure 6). Increased electronegativity led to more surface defects (WO_3-NWH-NaX and WO_3-NWH-KX series), whereas lower electronegativity, respectively stronger acidity led to surface defects abundance in the case of the WO_3-AMT-HX series. Analogous pattern was observed regarding each series: an increased proportion of surface defects resulted in improved photocatalytic efficiency.

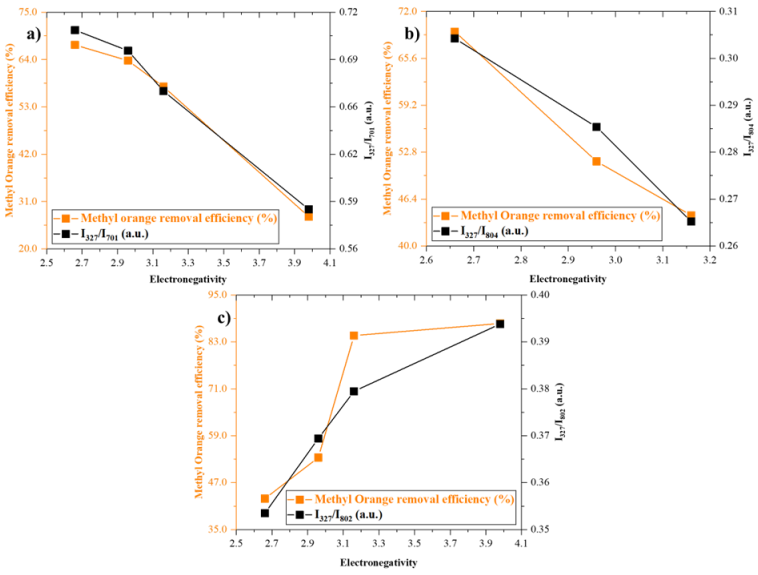

Figure 6. Influence of surface defects on TiO_2/WO_3 heterostructures photoactivity as a function of electronegativity a) WO_3-NWH-NaX; b) WO_3-NWH-KX; and c) WO_3-AMTHX series.

Optimization of TiO_2 to WO_3 ratio in TiO_2/WO_3 heterostructures for enhanced photocatalytic efficiency under UV light exposure

T4. Increased WO_3 percentage in TiO_2/WO_3 heterostructures influences the heterostructures optical and structural properties.

Different WO_3 percentage in the TiO_2/WO_3 heterostructures such as 1, 10, and 24 wt.% pseudo linearly diminished the E_g values of the composites, however higher WO_3 percentage (33% or 50%) did not influence the E_g values of the TiO_2/WO_3 heterostructures in the same way (Figure 7, b). The addition of 1 wt.% WO_3 to commercial TiO_2 shifted its E_g value to 3.14 eV; 10 wt.% WO_3 to 2.99 eV; 24 wt.% WO_3 to 2.76 eV; 33 wt.% WO_3 to 2.77 eV; and 50 wt.% WO_3 to 2.74 eV [48]. The composites FT-IR spectra revealed that, the vibrational bands directly linked to surface hydrophilicity, assigned to O─H vibrations located at 1630 and 3427 cm^{-1} were altered in response to the increased WO_3 percentage. These bands exhibited a relatively high intensity for composites containing 24 wt.% WO_3-AMT-HCl and a slight decreasing trend for samples containing less percentage of WO_3.

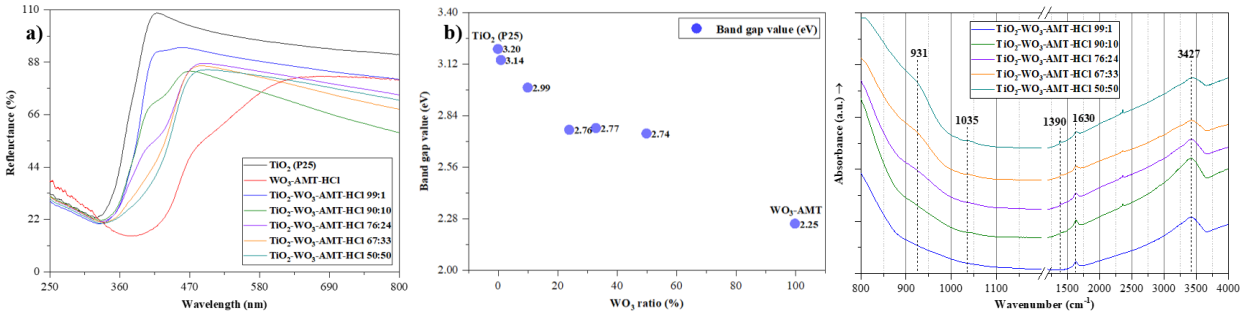

Figure 7. Optical and structural properties of TiO_2/WO_3 heterostructures with various TiO_2 to WO_3 ratios.

T5. Commercial TiO_2's photocatalytic performance can be enhanced by coupling it with WO_3 in various TiO_2 to WO_3 ratios.

Commercial TiO_2 is an efficient photocatalyst under UV light exposure, however its photocatalytic activity can be enhanced by coupling with metal oxides, in this particular case WO_3

metal oxides. The ratio of TiO_2 to WO_3 in the metal oxide composites is a paramount parameter, since certain ratios will inhibit the photocatalytic performance (Figure 8, left). TiO_2-WO_3-AMT-HCl 76:24 composite surpassed the reference photocatalysts' (TiO_2 removed 73.3%) removal efficiency, as it removed 99.0% of the pollutant. The 76:24 TiO_2 to WO_3 ratio was highly efficient in removing OA in various concentrations as it reached photodegradation rates above 95.0% in all cases, except when the OA concentration was the highest, in that case the photodegradation rate was 64.7% (Figure 8, right). The results prove that the photocatalytic efficiency of commercial TiO_2 can be enhanced in binary metal oxide composites.

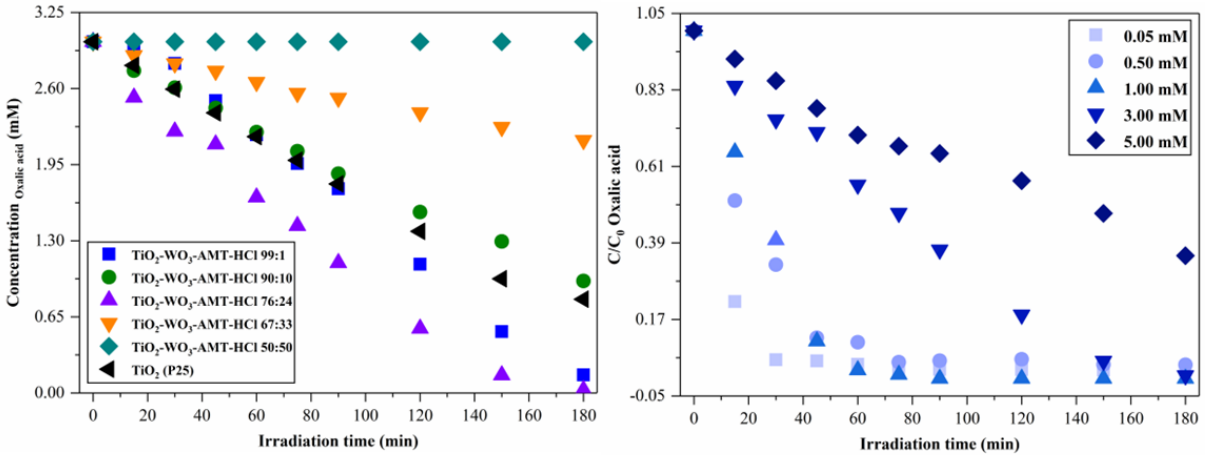

Figure 8. Photocatalytic removal of OA employing TiO_2/WO_3 heterostructures with various TiO_2 to WO_3 ratios (left); and photocatalytic efficiency of TiO_2-WO_3-AMT-HCl 76:24 composite in removing OA in various concentrations (right).

T6. TiO_2/WO_3 heterostructures possess the ability to detect and to remove pollutants simultaneously.

The response of the TiO_2-WO_3-AMT-HCl heterostructures as sensor (blue colorization of the suspension) is dependent on the pollutant concentration, and on the optical properties (color) of the heterostructures. Higher pollutant concentrations resulted in stronger sensor response. Qualitative detection of OA model pollutants in aqueous solutions can be a viable option for OA detection when the pollutant concentration is at least 5.00 mM since, in this case, the blue colorization of the suspension is observable with the naked eye (Figure 9). The data presented in

Figures 8 and 9 prove that TiO_2-WO_3-AMT-HCl heterostructures possess the ability to simultaneously detect and remove the OA model pollutant.

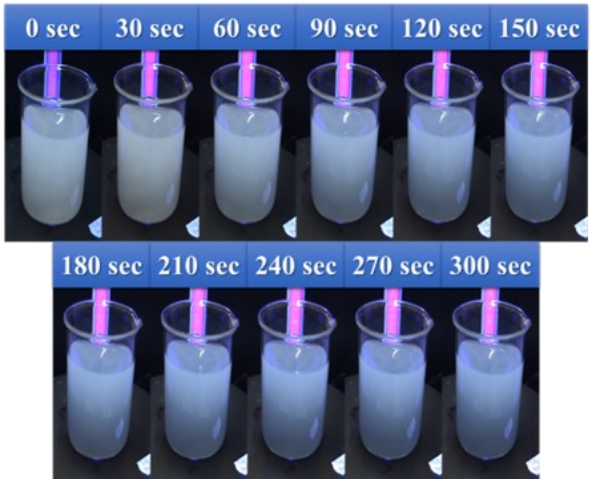

Figure 9. Detection of 5.00 mM OA under UV-A exposure employing TiO_2/WO_3-AMT-HCl heterostructures.

Optimization of TiO_2/WO_3 heterostructures *via* pH adjustment of the TiO_2-WO_3-AMT-HCl-WO_3-HW ternary composites for enhanced photocatalytic efficiency

T7. Structural investigations prove the presence of each component in the pH adjusted ternary composites.

In the previous thesis sub-chapters, it was proved that the optimal TiO_2 to WO_3 ratio was 76:24, so correspondingly the same ratio was used for the preparation of the novel ternary TiO_2/WO_3 heterostructures, but in this case two types of tungsten oxides (WO_3-HW and WO_3-AMT-HCl) were utilized in 12%-12% wt.% [49]. Since from the SEM micrographs the identification of each component of the ternary composites was not possible, structural investigations were carried out. The XRD patterns and the Raman spectra of the ternary composites proved the presence of each component in every sample (Figure 10). The heterostructures crystallinity deteriorated as the suspension medium was altered from strongly and moderately protonated to neutral and moderately deprotonated medium (Figure 10, left). The crystallinity

deterioration was possibly caused by the formation of amorphous Na_2WO_4 on the WO_3 semiconductors' surface, respectively to the intercalation of Na^+ into the crystal structure [50,51].

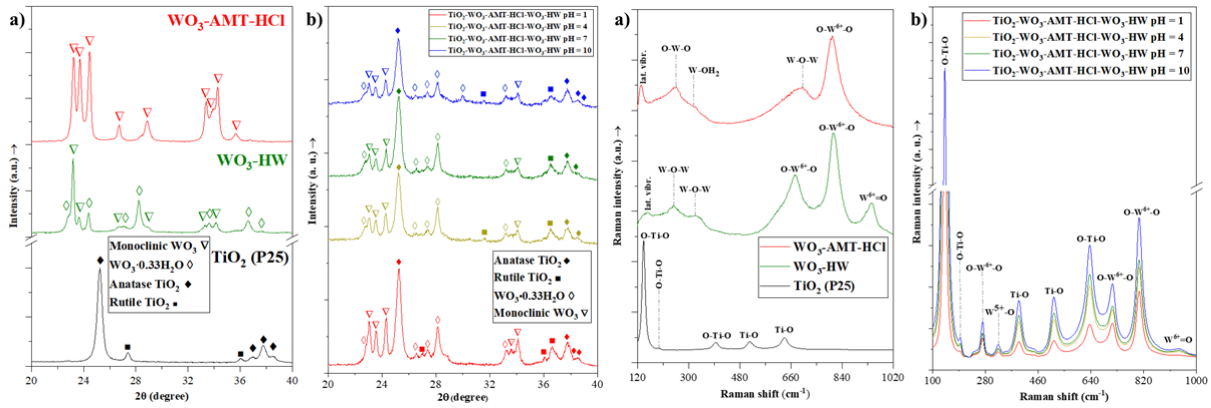

Figure 10. Structural properties of the individual metal oxides and the pH adjusted ternary heterostructures.

T8. The pH adjustment method for the preparation of ternary TiO_2/WO_3 heterostructures will result in composites with enhanced photoactivity.

Concerning OA photocatalytic degradation, composites with pH adjusted to 1 and 4 performed better than TiO_2 (47.9% efficiency), as they reached 95.9% and 72.2% OA removal efficiencies (Figure 11, left). The pH adjustment positively influenced two composites' photocatalytic efficiency in the case of OA photodegradation. Regarding MO decolorization rate, the photocatalytic performance of each pH-adjusted ternary composite was enhanced (Figure 11, right): they efficiently removed 97.0% of MO at pH = 1, 89.7% at pH = 4, 89.7% at pH = 7, and 98.7% at pH = 10. TiO_2 (P25) successfully removed 82.8% of MO.

Integrating two types of tungsten oxides, instead of the general one type of tungsten oxide, into the TiO_2/WO_3 composites *via* the pH adjustment method proved a viable option for preparing TiO_2/WO_3 heterostructures with enhanced photocatalytic performance. Integrating WO_3-AMT-HCl and WO_3-HW with MC and HPH crystalline phases into the TiO_2/WO_3 heterostructures had a synergic effect on the composites photoactivity due to the more effective charge carrier separation, inhibition of their recombination rate, and charge carriers' prolonged lifetime.

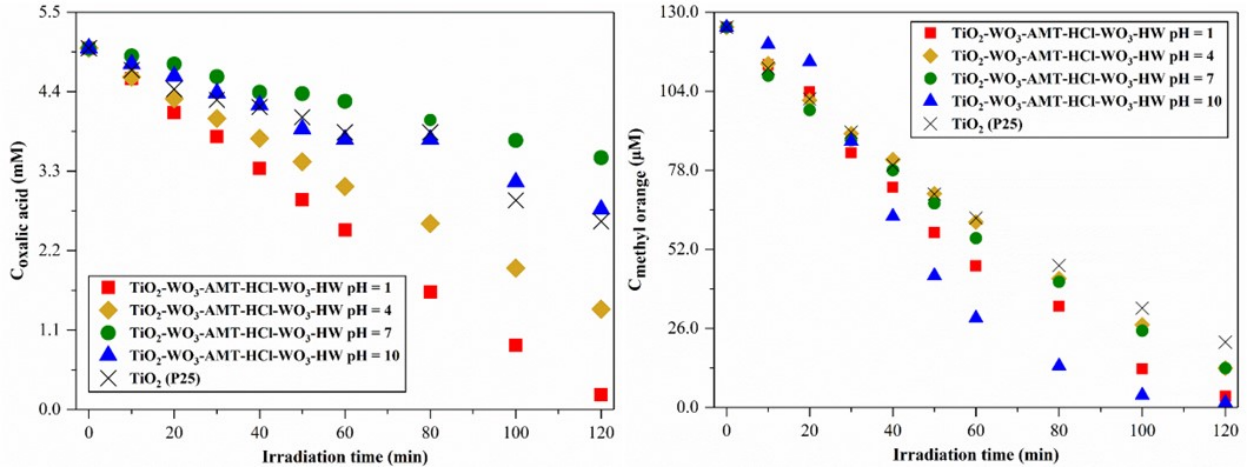

Figure 11. Photocatalytic degradation curves of OA (left) and MO (right) with the pH-adjusted ternary composites under UV light exposure.

T9. Correlations established between the pH-adjusted ternary composites' structural and optical parameters and their photocatalytic efficiencies.

It was observed that the pH adjusted ternary heterostructures' optical, structural and surface properties influenced their photocatalytic performance (Figure 12). The pH adjustment method led to the facet selective protonation or deprotonation of the TiO_2 and WO_3 semiconductors. The facet selective protonation or deprotonation in turn affected the ternary heterostructures crystallinity, E_g values, and surface defects. The ratio of WO_3-AMT-HCl (200) to TiO_2-A (101), correspondingly the ratio WO_3-AMT-HCl (200) to WO_3-HW (220) influenced the heterostructures photocatalytic performance in the same manner: lower ratios led to lower photocatalytic efficiencies, whereas higher ratios led to enhanced photocatalytic efficiencies. WO_3 surface defects also influenced the heterostructures photocatalytic performance: surface defects abundance inhibited the composites photocatalytic activity. From the data presented, it can be concluded, that the photocatalytic efficiency of TiO_2/WO_3 heterostructures can be significantly improved by integrating two WO_3 metal oxides with different geometries and crystalline phases, respectively by employing the pH adjustment method to obtain ternary TiO_2/WO_3 heterostructures.

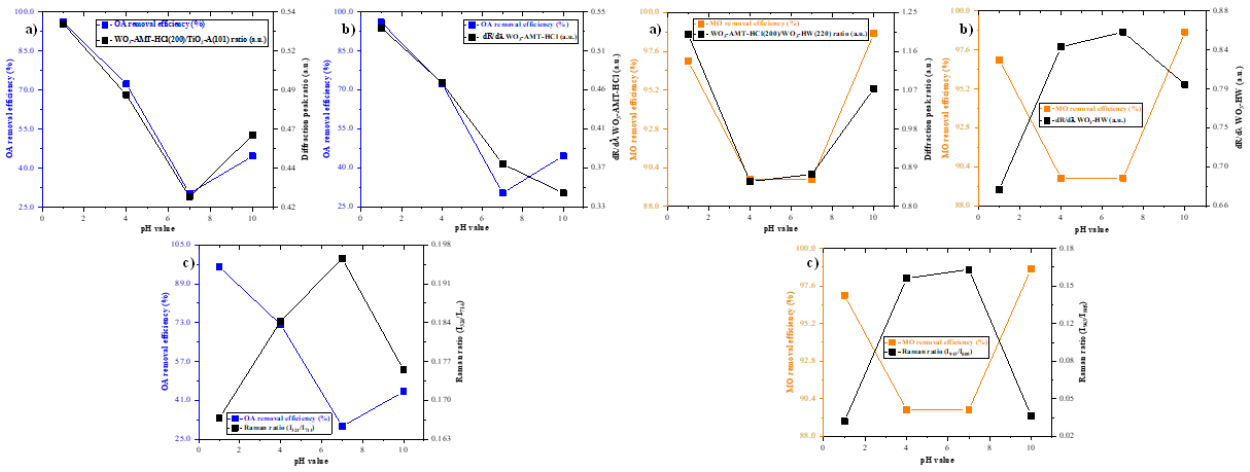

Figure 12. Correlations established between the pH-adjusted ternary composites' structural and optical parameters and their efficiency regarding OA (left) and MO (right) photocatalytic removal.

Electron trapping in TiO_2/WO_3-NWH-NaCl, TiO_2-WO_3-AMT-HCl heterostructures for applications in AOPs and sensing

T10. Charge transfer in TiO_2/WO_3-NWH-NaCl heterostructures (ethanol – EtOH – vapor detection under brief UV light irradiation).

The applicability of tungsten oxides as sensors, particularly hydrated types of tungsten oxides in TiO_2/WO_3 composites, is related to the capability of W^{6+} species to be reduced to W^{5+}. This reduction is the result of the electron transfer from TiO_2 to WO_3-NWH-NaCl (Figure 13). In the presence of molecular oxygen atoms, the reduced W^{5+} species will be oxidized, and they return to their original W^{6+} states [52].

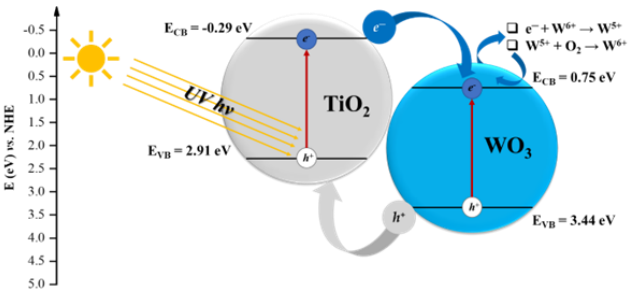

Figure 13. Charge transfer mechanism in TiO_2/WO_3-NWH-NaCl heterostructures.

T11. The photocatalytic performance of TiO_2/WO_3 heterostructures can be improved through the simple suspension preparation method.

TiO_2/WO_3-NWH-NaCl and TiO_2/WO_3-AMT-HCl heterostructures were prepared *via* the simple suspension method in the well-established 76:24 TiO_2 to WO_3 ratio. The photocatalytic activity of the composites was assessed by the removal of OA and MO model pollutants under UV light irradiation. Concerning OA photodegradation the obtained TiO_2/WO_3-NWH-NaCl and TiO_2/WO_3-AMT-HCl heterostructures did not performed better than the reference photocatalyst (TiO_2), as they reached OA removal rates of 75.5% and 77.2%, whereas TiO_2 reached a 95.7% removal efficiency (Figure 14, left). Regarding MO decolorization rate, the simple suspension preparation method led to improved photocatalytic efficiencies in the case of both composites. Commercial TiO_2 reached an 82.8% decolorization rate, TiO_2/WO_3-AMT-HCl and TiO_2/WO_3-NWH-NaCl heterostructures reached 88.9% and 96.7% decolorization rates (Figure 14, right). The results presented here prove that the photocatalytic performance of TiO_2/WO_3 composites can be efficiently improved by employing a simple and straightforward preparation method. The improved photocatalytic performance of TiO_2/WO_3 composites was attributed to the synergistic effect between TiO_2 and WO_3 metal oxides, which resulted in more efficient charge carrier separation and a lower recombination rate.

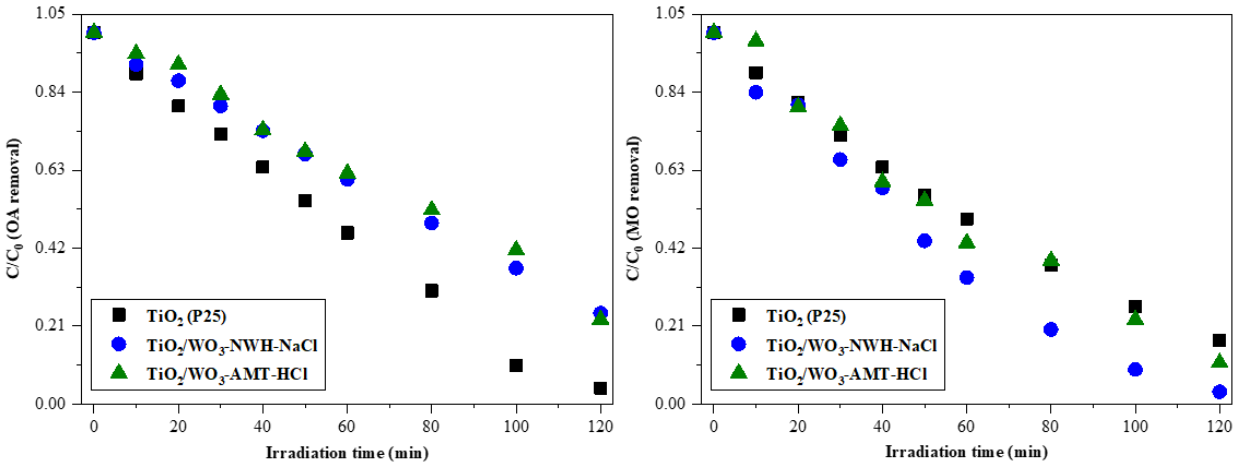

Figure 14. Photocatalytic removal of OA (left) and MO (right) solutions under UV light exposure employing commercial TiO_2 and TiO_2/WO_3 composites.

T12. TiO_2/WO_3 heterostructures sensory applicability in closed and open systems (EtOH detection under UV light exposure; OA detection under direct sunlight).

The TiO_2/WO_3 heterostructures applicability as sensors in closed systems was carried out by assessing the heterostructures ability to detect EtOH vapors after a short (15 minutes) UV light exposure (Figure 15). To assess the heterostructures sensing capabilities their reflectance spectra were recorded prior to the UV light exposure, and afterwards to a span of 70 minutes. The difference in relative intensities of the reflectance spectra between the unexposed and UV-exposed TiO_2/WO_3-NWH-NaCl composite, which can be ascribed to the direct reduction process of W^{6+} species to W^{5+}, was found to be 73.7% (Figure 15, right). Conversely, in the case of TiO_2/WO_3-AMT-HCl composites, this difference in reflectance relative intensities was determined to be 37.9% (Figure 15, left). The stronger sensor response exhibited by the TiO_2/WO_3-NWH-NaCl heterostructures, as compared to the TiO_2/WO_3-AMT-HCl heterostructures, can be attributed to the increased percentage of W^{5+} species present in the WO_3-NWH-NaCl metal oxides (4.1%) that of the WO_3-AMT-HCl metal oxides (2.4%). The data presented here indicate that TiO_2/WO_3-NWH-NaCl heterostructures can function as effective vapor sensors in closed systems due to their fast and stronger sensor response.

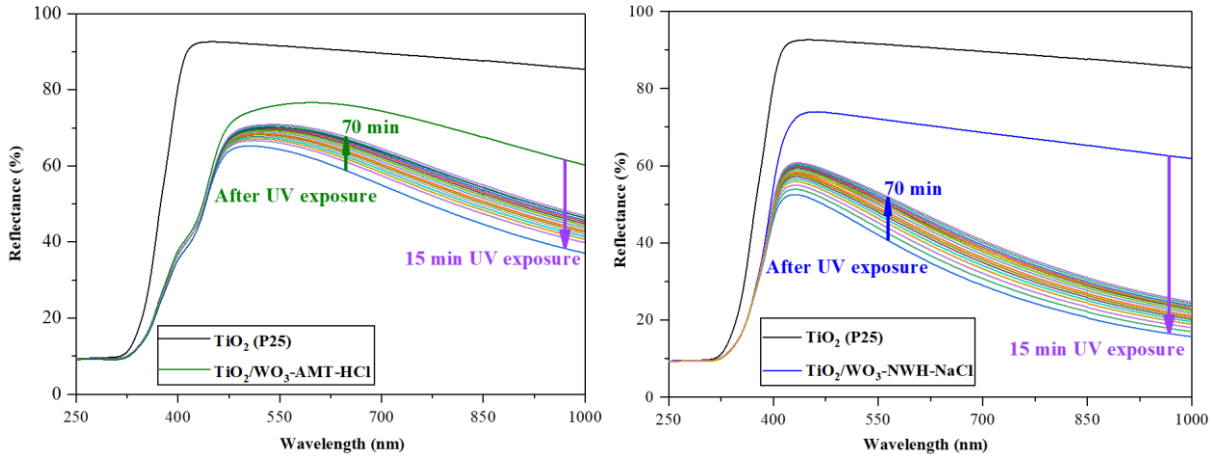

Figure 15. Reflectance spectra of TiO_2/WO_3-AMT-HCl and TiO_2/WO_3-NWH-NaCl composites before and after UV exposure (EtOH vapor detection).

The assessment of the sensorial applicability of TiO_2/WO_3 heterostructures in open systems was conducted through the drop-wise addition of a 1 mL solution of OA (5 mM) onto the side of

the tin foil that was coated with TiO_2. Following the application of a coating onto the tin foil, the exposed surface (containing TiO_2) was subjected to direct sunlight (Figure 16). Subsequently, the side with the WO_3 metal oxides promptly exhibited a distinct blue hue. The information presented in this section prove that TiO_2/WO_3 heterostructures with different geometries and crystalline phases can be employed successfully for the photocatalytic removal of several pollutants, and as sensor in closed and open systems under UV light or direct sunlight exposure.

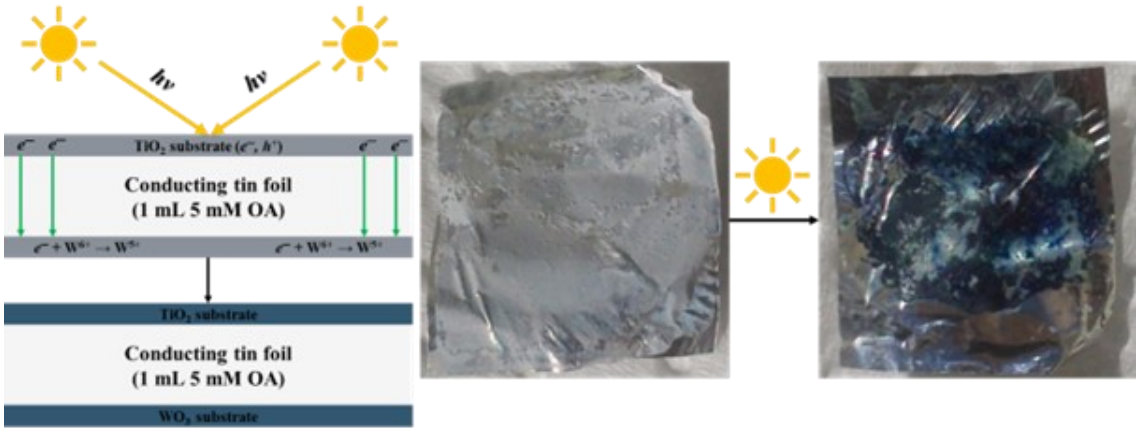

Figure 16. Application of TiO_2/WO_3 heterostructures as sensor for OA detection in open systems.

Applications in heterogeneous photocatalysis and surface-enhanced Raman spectroscopy of WO_3 and $WO_3 \cdot 0.33H_2O$ morphology-dependent $Au/TiO_2/WO_3$ heterojunctions

T13. Synthesis and morphology investigations of the $Au/TiO_2/WO_3$ heterojunctions.

For the synthesis of the tungsten oxide morphology dependent $Au/TiO_2/WO_3$ heterojunctions, three different WO_3 geometries were selected: prismatic (WO_3-HW), rod-like (WO_3-NWH), and flower-like (WO_3-AMT). Au NPs were deposited on the TiO_2/WO_3 heterostructures surface *via* a slightly altered Turkevich-Frens methods. Au NPs were deposited either by the heat-assisted method or by the time-assisted method. The average Au NPs' size in each case was approximatively 20 nm (Figure 17). Time assisted deposition method resulted in

the successful deposition of Au NPs in higher percentages regardless of the WO_3 morphology [53]. The deposited Au NPs' geometry was spherical, regardless of the deposition method or WO_3 morphology. Au/TiO_2/WO_3 heterojunctions were successfully obtained by employing the slightly altered Turkevich-Frens Au NPs deposition methods (Figure 17).

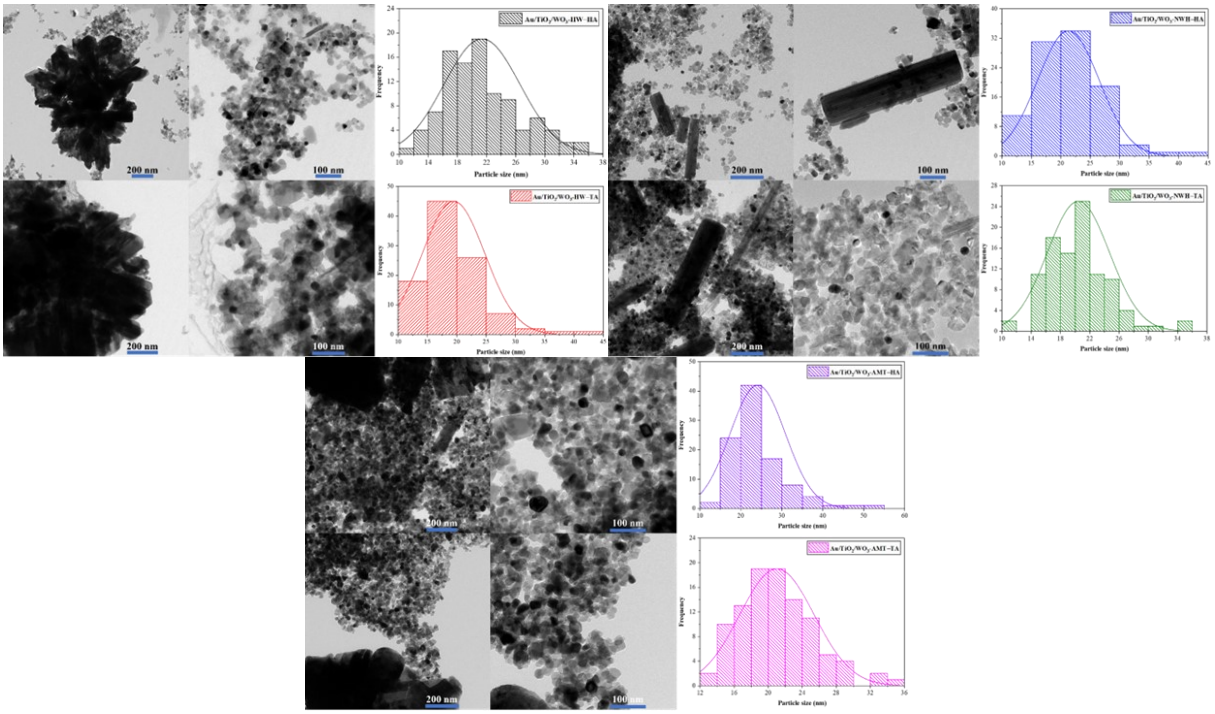

Figure 17. Au/TiO_2/WO_3 heterojunctions' TEM micrographs and the deposited Au NP's distribution histograms.

T14. Photocatalytic recyclability and stability of the Au/TiO_2/WO_3 heterojunctions.

The stability and recyclability of Au/TiO_2/WO_3 heterojunctions were investigated over three photodegradation cycles for each model pollutant (Figure 18, left). The composites demonstrating the highest photocatalytic performance were selected for evaluation in terms of their potential for recyclability. The stability of the composites was evaluated by recording the FT-IR spectra of the samples before and after undergoing photodegradation (Figure 18, right). Based on the analysis of the photocatalysts' FT-IR spectra following three reutilization cycles, no significant alterations were observed, except for minor modifications observed in the absorption bands associated with adsorbed water molecules (Figure 18, right). The synthesized Au/TiO_2/WO_3

heterojunctions proved to be highly stable even after several recycling rounds and are viable photocatalysts since their photocatalytic performance diminished only slightly after three recycling rounds.

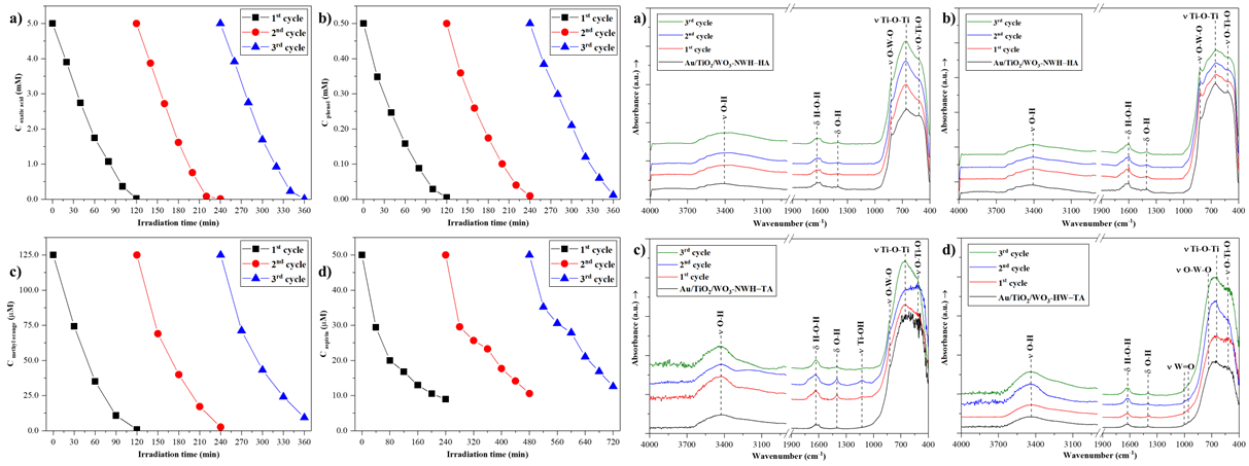

Figure 18. Au/TiO_2/WO_3 heterojunctions' reusability up to three photodegradation cycles (left); and Au/TiO_2/WO_3 heterojunctions' stability (right) after several cycles of reusability as shown by FT-IR spectra.

T15. Crystal violet dye detection on Au/TiO_2/WO_3 substrates using SERS, and durability of Au/TiO_2/WO_3 heterojunctions as SERS substrates.

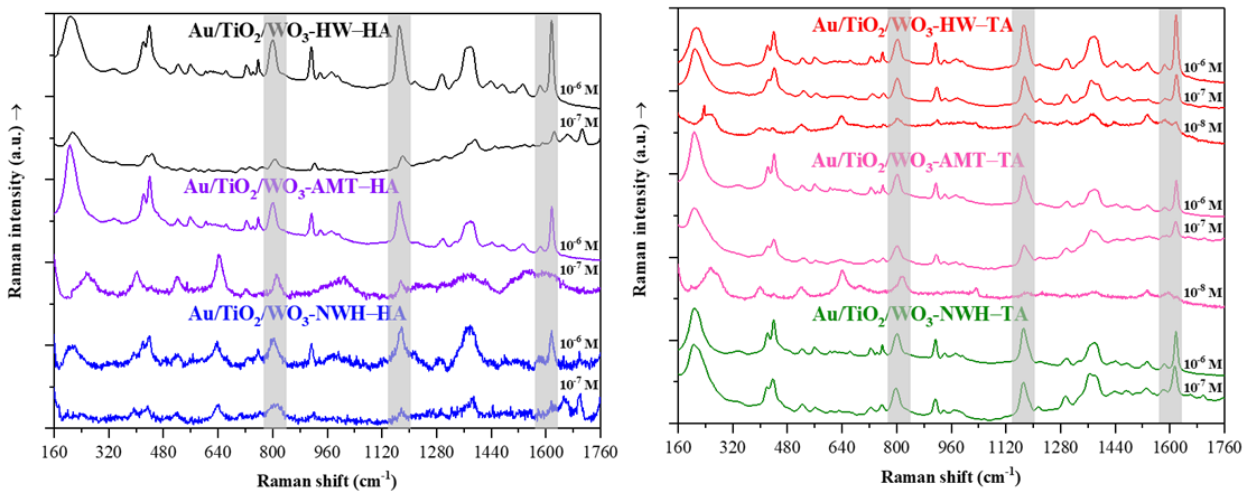

Figure 19. The detection limit of crystal violet dye adsorbed on various Au/TiO_2/WO_3 substrates.

Crystal violet was successfully detected on the $Au/TiO_2/WO_3$ substrates at concentrations as low as 10^{-6} M, 10^{-7} M, and 10^{-8} M. Specific crystal violet SERS bands were observed in each recorded SERS spectra (Figure 19). Upon analysis of the SERS spectra, it is discernible that certain heterojunctions exhibit a superior enhancement of the Raman signal compared to others. This difference was linked to the Au NP's morphology and particle size [54]. Through a comprehensive analysis of the SERS spectra of crystal violet on $Au/TiO_2/WO_3$ substrates, it was concluded that the heterostructures $Au/TiO_2/WO_3$-HW─TA and $Au/TiO_2/WO_3$-AMT─TA were the most promising ones, as their detection limit for crystal violet was 10^{-8} M. In order to evaluate the stability of $Au/TiO_2/WO_3$ heterojunctions as SERS substrates, the SERS spectra of the crystal violet molecule adsorbed on $Au/TiO_2/WO_3$-HW─TA and $Au/TiO_2/WO_3$-AMT─TA substrates with varying concentrations (ranging from 10^{-6} to 10^{-8} M), were re-recorded after 4 years (Figure 20). The strong intensity of the SERS signal and the photocatalytic recycling tests prove the extraordinary stability of the $Au/TiO_2/WO_3$ heterojunctions.

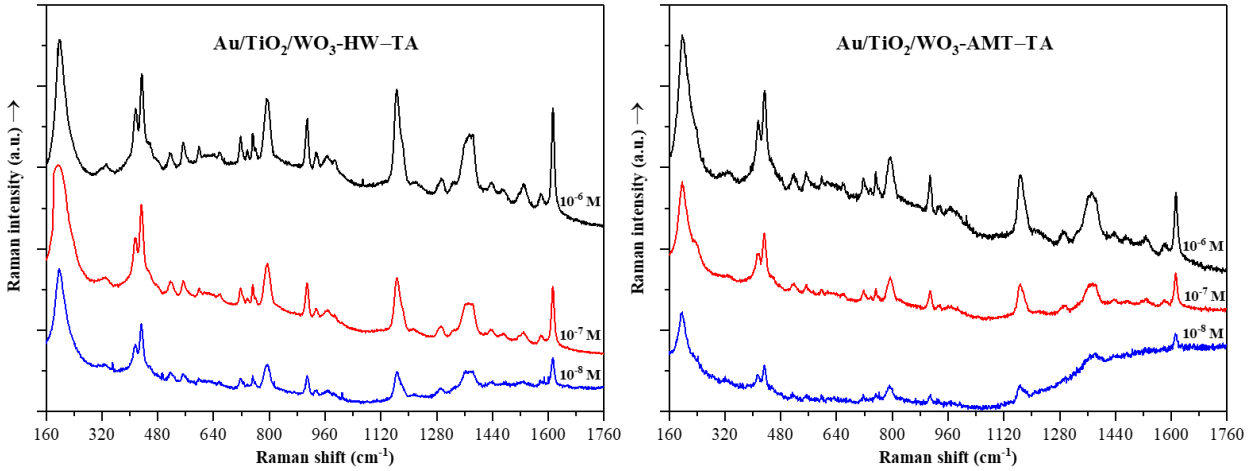

Figure 20. Newly recorded SERS spectra (after 4 years) of crystal violet adsorbed on $Au/TiO_2/WO_3$-HW─TA (left) and $Au/TiO_2/WO_3$-AMT─TA (right) substrates at different concentrations.

5. Conclusions

The aim of the thesis was to obtain tungsten oxide-based semiconductors with different morphologies and crystalline phases and to assess their photocatalytic efficiently for removing several model pollutants as well as their ability as sensors for detecting chemical contaminants. The morpho-structural properties of synthesized semiconductors have been studied. A successful synthesis design of hydrothermal crystallization routes for obtaining shape-tailored tungsten oxide semiconductors has been presented. The influence of synthesis parameters on the WO_3 semiconductors' morphology, structure, and optical properties has been studied.

The synthesized metal oxides were inactive in photocatalytic experiments, likely due to fast charge carrier recombination. The problem was addressed by preparing TiO_2/WO_3 heterostructures and utilizing them as photocatalysts to remove pollutants under UV light. The TiO_2/WO_3 composites were prepared by mixing commercial TiO_2 with flower/star-like 100% MC WO_3 (WO_3-AMT-HCl). The optimal composition was 76% TiO_2 and 24% WO_3. Under UV light irradiation for 3 hours, the TiO_2/WO_3 heterostructures removed 99% of a 3 mM OA solution, while commercial TiO_2 removed 73.3% of the pollutant. The composites' photocatalytic performance was linked to the heterostructures' water affinity, showing a correlation between hydrophilicity and photocatalytic activity. The TiO_2/WO_3-AMT-HCl samples have been used as a sensor to detect OA in concentrations from 0.05 to 5.00 mM. The sensorial applicability of TiO_2/WO_3 was due to the reduction of W^{6+} to W^{5+} in WO_3 and the charge transfer mechanism between TiO_2 and WO_3.

To study the combined effect of differently shaped tungsten oxides and pH adjustment on the TiO_2/WO_3 composites' photocatalytic performance, TiO_2/WO_3 heterostructures were prepared using an alternative approach. The ratio of TiO_2 to WO_3 remained the same (76:24), but two types of WO_3 metal oxides were added to the composites in a 12-12 wt.% proportion. The suspensions' pH adjustment method was used to prepare the heterostructures. The pH adjustment influenced the crystallinity of the heterostructures. Alkaline conditions had a negative effect, while protonated conditions had a positive effect. Surface defects were induced by this method for TiO_2/WO_3 preparation. W^{5+} species were detected in the Raman spectra of the samples, and they directly impacted the photocatalytic performance of the heterostructures. The pH adjustment method improved photocatalytic performance for specific pollutants, proving the synergic effect of two types of WO_3 metal oxides in the TiO_2/WO_3 systems.

Additionally, TiO_2/WO_3 heterostructures were prepared using the simple suspension method. The composites' ratio was 76:24 in this case too. The TiO_2/WO_3 heterostructures composites removed 77.2% of OA after 2 hours. TiO_2/WO_3-AMT-HCl achieved 88.9% MO decolorization after 2 hours, while TiO_2/WO_3-NWH-NaCl achieved 96.7% MO decolorization. The previous TiO_2/WO_3-AMT-HCl heterostructures have been used to detect OA. The sensing abilities of TiO_2/WO_3-AMT-HCl and TiO_2/WO_3-NWH-NaCl heterostructures to detect EtOH vapors in a sealed vial under UV light exposure were examined. Both composites efficiently detected EtOH vapors, but the TiO_2/WO_3-NWH-NaCl composite exhibited a more intense blue colorization. The TiO_2/WO_3-NWH-NaCl heterostructures had a stronger sensor response due to the HPH phase of WO_3-NWH-NaCl semiconductors, more surface OH, and a higher percentage of W^{5+} species (4.0%) in bulk compared to WO_3-AMT-HCl semiconductors (2.4%).

$Au/TiO_2/WO_3$ heterostructures were synthesized *via* modified Turkevich-Frens routes: HA and TA—the desired heterojunction composition was: 1% Au, 24% WO_3, and 75% TiO_2. The photocatalytic performance of the heterojunctions in removing OA, PHE, MO under UV light exposure, and ASP under Vis light exposure was evaluated. The best-performing heterojunctions were $Au/TiO_2/WO_3$-NWH─HA, $Au/TiO_2/WO_3$-NWH─TA, and $Au/TiO_2/WO_3$-HW─TA. They removed 96.6% of OA, 99.0% of PHE, and 97.9% of MO dye under UV light. Under Vis light exposure, they removed 82.1% of ASP. The heterojunctions were employed as SERS substrates for detecting crystal violet dye down to nanomolar concentrations. The heterojunctions were stable and recyclable after multiple utilization cycles. $Au/TiO_2/WO_3$-HW─TA and $Au/TiO_2/WO_3$-AMT─TA heterojunctions had the highest Au content and achieved a crystal violet detection limit of 10^{-8} M.

This research produced multiple WO_3 semiconductors with diverse morphologies and properties. The hydrothermally crystallized WO_3 materials were inactive photocatalysts for multiple pollutants under UV or Vis irradiation. The TiO_2/WO_3 composites, prepared through various methods such as mechanical mixing, pH adjustment, or suspension, were more efficient than TiO_2 in removing model pollutants under UV light exposure. TiO_2/WO_3 composites could detect OA solutions and EtOH vapors in closed systems and function as sensors in open systems. The $Au/TiO_2/WO_3$ heterojunctions showed improved photocatalytic performance (compared to TiO_2) for various pollutants under UV and Vis light. $Au/TiO_2/WO_3$ heterojunctions detected

crystal violet dye at 10^{-8} M and remained stable as SERS substrates, providing strong signals even after 4 years.

6. Scientific activity

List of publications related to the Ph.D. thesis

ISI rated journals

1. B. Boga, **I. Székely**, Z. Pap, L. Baia, M. Baia, "*Detailed Spectroscopic and Structural Analysis of TiO_2/WO_3 Composite Semiconductors"*, Journal of Spectroscopy, 2018, (Web of Science, IF: 1.376, AIS: 0.249); 19 citations (Google Scholar);
2. **I. Székely**, M. Baia, K. Magyari, B. Boga, Z. Pap, "*The effect of the pH adjustment upon the WO_3-$WO_3 \cdot 0.33H_2O$-TiO_2 ternary composite systems' photocatalytic activity"*, Applied Surface Science, 2019, (Web of Science, IF: 6.182, AIS: 0.772); 12 citations (Google Scholar);
3. **I. Székely**, E.Z. Kedves, Z. Pap, M. Baia, "*Synthesis Design of Electronegativity Dependent WO_3 and $WO_3 \cdot 0.33H_2O$ Materials for a Better Understanding of TiO_2/WO_3 Composites' Photocatalytic Activity*", Catalysts, 2021, (Web of Science, IF: 4.501, AIS: 0.615); 7 citations (Google Scholar);
4. B. Boga, **I. Székely**, M. Focșan, M. Baia, T. Szabó, L. Nagy, Z. Pap, "*Sensor surface via inspiration from Nature: The specific case of electron trapping in $TiO_2/WO_3(\cdot 0.33H_2O)$ and reaction center/$WO_3(\cdot 0.33H_2O)$ systems*", Applied Surface Science, 2022, (Web of Science, IF: 6.70, AIS: 0.865); 3 citations (Google Scholar);
5. **I. Székely**, Z. Kovács, M. Rusu, T. Gyulavári, M. Todea, M. Focșan, M. Baia, Z. Pap, "*Tungsten oxide morphology-dependent $Au/TiO_2/WO_3$ heterostructures with applications in heterogenous photocatalysis and surface-enhanced Raman spectroscopy*", Catalysts, 2023, (Web of Science, IF: 3.9, AIS: 0.591); no citations (Google Scholar).

List of conference presentations related to the Ph.D. thesis

International conferences

1. **I. Székely**, B. Boga, G. Kovács, Z. Pap, K. Hernádi, L. Baia. M. Baia, "*Assessment of photocatalytic and organic pollutant detection properties of TiO_2-WO_3 nanocomposite systems*", Poster presentation, 5th European Conference on Environmental Applications of Advanced Oxidation Processes (EAAOP5), Prague, Czech Republic, 2017.

2. M. Baia, L. Baia, **I. Székely**, Z. Pap, "*Ionic strength upon the structure and morphology of WO_3 semiconductors. Study of WO_3 and WO_3-TiO_2 composites photoactivity*", Poster presentation, 3rd World Congress on Materials Science & Engineering, Barcelona, Spain, 2017.
3. **I. Székely**, M. Baia, Z. Pap, K. Hernádi, "*The effect of the pH adjustment upon the WO_3-$WO_3 \cdot 0.33H_2O$-TiO_2 ternary composite systems' photocatalytic activity*", Oral presentation, **Augustin Maior Prize for Best Oral presentation**, 12th International Conference on Physics of Advanced Materials (ICPAM-12), Heraklion, Crete, Greece, 2018.
4. **I. Székely**, M. Baia, Z. Pap, K. Hernádi, "*Inducing surface defects in WO_3-$WO_3 \cdot 0.33H_2O$-TiO_2 ternary composites and their photocatalytic efficiency for model pollutants removal*", Poster presentation, 6th European Conference on Environmental Applications of Advanced Oxidation Processes (EAAOP6), Portoroz, Slovenia, 2019.
5. **I. Székely**, E.Z. Kedves, M. Baia, Z. Pap, "*The impact of different anions and cations electronegativity on WO_3's morphological, structural and photocatalytic properties*", Poster presentation, 2021 Spring Meeting of the European Materials Research Society (E-MRS), Virtual Conference, Strasbourg, France, 2021.
6. **I. Székely**, M. Rusu, M. Baia, Z. Pap, "*Applications of $Au/TiO_2/WO_3$ ternary composite systems as SERS materials and photocatalysts*", Oral presentation, 11th International Conference on Advanced Vibrational Spectroscopy (ICAVS 11), Online Conference, Kraków, Poland, 2021.
7. **I. Székely**, K. Saszet, M. Rusu, T. Gyulavári, M. Baia, Z. Pap, "*$Au/TiO_2/WO_3$ composites' multiple applicability as photocatalysts and SERS materials*", Oral presentation, 13th International Conference on Physics of Advanced Materials (ICPAM-13), Hybrid Conference, Sant Feliu de Guixols, Spain, 2021.
8. **I. Székely**, M. Rusu, M. Baia, Z. Pap, "*Synthesis of a multifunctional $Au/TiO_2/WO_3$ composite with multiple applications in heterogeneous photocatalysis*", Mini-oral presentation, 5th EuChemS Conference on Green and Sustainable Chemistry (5th EuGSC), Virtual Conference, Thessaloniki, Greece, 2021.
9. **I. Székely**, K. Saszet, Zs-R. Tóth, T. Gyulavári, K. Magyari, M. Baia, "*Synergistic effect of monoclinic and partially hydrated WO_3 in $Au/TiO_2/WO_3$-$WO_3 \cdot 0.33H_2O$*

heterostructures for applications in heterogenous photocatalysis and SERS", Oral presentation, 14th International Conference on Physics of Advanced Materials (ICPAM-14), Hybrid Conference, Dubrovnik, Croatia, 2022.

National conferences

1. **I. Székely**, B. Boga, A. Csavdári, G. Kovács, Z. Pap, M. Baia, K. Hernádi, "*A Novel WO_3-TiO_2 Based Composite Semiconductors: Synthesis, Morpho-structural Analysis and Photocatalytic Activity Assessment*", Oral presentation, XXII. International Conference on Chemistry, Timișoara, Romania, 2016.
2. **I. Székely**, B. Boga, A. Csavdári, G. Kovács, Z. Pap, M. Baia, K. Hernádi, "*Application of WO_3-TiO_2 based semiconductor nanomaterials as photocatalysts for the removal of dyes*", Oral presentation, Transylvanian Museum Association, ETK-17, Cluj-Napoca, Romania, 2017.

List of other publications

ISI rated journals

1. N. Sharma, Z. Pap, **I. Székely**, M. Focșan, G. Karacs, Z. Nemeth, S. Garg, K. Hernádi, "*Combination of iodine-deficient BiOI phases in the presence of CNT to enhance photocatalytic activity towards phenol decomposition under visible light*", Applied Surface Science, 2021, (Web of Science, IF: 7.392, AIS: 0.848); 20 citations (Google Scholar);
2. K. Magyari, A. Dreancă, **I. Székely**, A. Popescu, A. Feraru, E. Páll, T. Gyulavári, M. Suciu, M. Cenariu, E. Bobu, L. Baia, M. Baia, "*How does the structure of pullulan alginate composites change in the biological environment?"* Journal of Materials Science, 2022, (Web of Science, IF: 4.50, AIS: 0.627); 1 citation (Google Scholar);
3. Zs-R. Tóth, D. Debreczeni, T. Gyulavári, **I. Székely**, M. Todea, G. Kovács, M. Focșan, K. Magyari, L. Baia, Z. Pap, K. Hernádi, "*Rapid Synthesis Method of Ag_3PO_4 as Reusable Photocatalytically Active Semiconductor*", Nanomaterials, 2023, (Web of Science, IF: 5.30, AIS: 0.707); 3 citations (Google Scholar);

4. A. G. Mihiș, L. C. Coteț, C. Cadar, L. C. Pop, M. Todea, M. M. Rusu, A. Vulpoi, **I. Székely**, C. A. Sălăgean, K. Magyari, M. Mureșan-Pop, O. Cadar, M. Baia, I. E. Sofran, G. Lisa, I. Anghel, M. Baibarac, V. Danciu, L. Baia, *"Structural and flame retardancy properties of GO-DOPO-HAK composite"*, Journal of Materials Science, 2023, (Web of Science, IF: 4.50, AIS: 0.627); 0 citations (Google Scholar);
5. B. Boga, V-M. Cristea, **I. Székely**, F. Lorenz, T. Gyulavári, L. C. Pop, L. Baia, Z. Pap, N. Steinfeldt, J. Strunk, *"Experimental data-driven and phenomenological modeling approaches targeting the enhancement of $CaTiO_3$ photocatalytic efficiency"*, Sustainable Chemistry and Pharmacy, 2023, (Web of Science, IF: 6.00, AIS: 0.640); 1 citation (Google Scholar);
6. E-Z. Kedves, C. Fodor, Á. Fazekas, **I. Székely**, Á. Szamosvölgyi, A. Sápi, Z. Kónya, L. C. Pop, L. Baia, Z. Pap, *"α-MoO_3 with inhibitive properties in Fenton reactions and insights on its general impact on OH radical based advanced oxidation processes"*, Applied Surface Science, 2023, (Web of Science, IF: 6.70, AIS: 0.865); 3 citations (Google Scholar).

Non-ISI journals

1. E.Z. Kedves, **I. Székely**, L. Baia, M. Baia, A. Csavdári, Z. Pap, "*The Comparison of the Photocatalytic Performance Shown by TiO_2 and TiO_2/WO_3 Composites — A Parametric and Kinetic Study*", Journal of Nanoscience and Nanotechnology, 2019, (Web of Science, IF: 1.134, AIS: 0.142); 8 citations (Google Scholar);
2. L.C. Coteț, C. Cadar, A. Mihiș, K. Magyari, M. Mureșan-Pop, L.C. Pop, A. Mihăilă, **I. Székely**, S. Drăgan, M. Dudescu, I. Zgura, E. Matei, M. Baia, M. Baibarac, I. Anghel, L. Baia, "*Mixture of Graphene Oxide/Phosphoric Acid/Melamine as Coating for Improved Fire Protective Performance and Enhancement of Surface Electrical Properties on Wood Chipboard*", Journal of Nanoscience and Nanotechnology, 2021, (Web of Science, IF: 1.134, AIS: 0.142); 4 citations (Google Scholar);
3. A. Mihiș, V. Danciu, C. A. Sălăgean, **I. Székely**, M. V. Racolța-Paina, S. C. Tripon, L. C. Coteț, K. Magyari, L. Baia, *"The effect of alkali and surfactant concentration,*

temperature and stirring on the cleaning efficiency of the carbon steel surface", Studia UBB Physica, 2021, (BDI, IF: -, AIS: -); 2 citations (Google Scholar);

4. L. C. Coteț, C. Sălăgean, A. Mihiș, **I. Székely**, Zs. Tóth, L. Baia, M. Baia, G. Olteanu, I. Olteanu, V. Danciu, *"Suspension Based on a Mixture of Titania-Silica-Functionalized Graphene Oxide for Surface Consolidation of Historical Andesite Stone and Mortar"*, Studia UBB Physica, 2021, (BDI, IF: -, AIS: -); 0 citations (Google Scholar).

List of other conference presentations

International conferences

1. B. Boga, **I. Székely**, K. Hajdu, G. Kovács, Z. Pap, M. Baia, K. Hernádi, L. Nagy, "*Bioelectronic and photocatalytic application of composite systems based on WO_3 and mathematical modelling of oxalic acid degradation using WO_3/TiO_2 composites*", Oral presentation, *Supervisor*, 15th International Conference "Students for Students", Cluj-Napoca, Romania, 2019.
2. N. Sharma, Z. Pap, S. Garg, K. Hernádi, **I. Székely**, "*Investigating role of $Bi_6O_6(OH)_3(NO_3)_3 \cdot 1.5H_2O$ as intermediate compound in BiOBr/MWCNT composites with (003) facet favoring phenol degradation under visible light*", Poster presentation, 6th European Conference on Environmental Applications of Advanced Oxidation Processes (EAAOP6), Portoroz, Slovenia, 2019.
3. B. Boga, M-V. Cristea, T. Gyulavári, **I. Székely**, Z. Pap, "*Modeling and Optimizing the Photocatalytic Efficiency of Hydrothermally Obtained $CaTiO_3$ via Polynomial Regression and Artificial Neural Network Models*", Oral presentation, *Supervisor*, 17th International Conference "Students for Students", Cluj-Napoca, Romania, 2021.
4. B. Boga, M-V. Cristea, **I. Székely**, Z. Pap, "*Hydrothermal Synthesis of $CaTiO_3$ and Photocatalytic Performance Optimization Using Statistical Models*", Oral presentation, *Supervisor*, 22nd Technical Scientific Student Conference, Timișoara, Romania, 2021, (1st Place Prize).
5. B. Boga, **I. Székely**, T. Gyulavári. M-V. Cristea, Z. Pap, "*Synthesis design of $CaTiO_3$ and the assessment of photoreactor design parameters*", Oral presentation, *Supervisor*,

5th EuChemS Conference on Green and Sustainable Chemistry (5th EuGSC), Virtual Conference, Thessaloniki, Greece, 2021.

6. Fodor C., Kedves E.-Z., **Székely I**., Pop L.-C., Baia L. "*Preparation of α-MoO3 with different crystallographic plane ratios: study of the adsorption process using organic dyes*", Oral presentation, 9th European Young Engineers Conference, Online Conference, Warsaw, Poland, 2021.
7. K. Magyari, A. Dreanca, **I. Székely**, E. Bobu, E. Páll, M. Cenariu, L. Baia, M. Baia, "*In Vitro Bioactivity and Biocompatibility of Alginate-Pullulan Based Composites*", Oral presentation, New Trends in Polymer Science: Health of the Planet, Health of the People, Turin, Italy, 2022.
8. B. Boga, N. Steinfeldt, V. Cristea, F. Lorenz, **I. Székely**, T. Gyulavári, Z. Pap, J. Strunk, "*Correlation between hydrothermal synthesis conditions – morpho-structural peculiarities – photocatalytic efficiency of $CaTiO_3$ and $SrTiO_3$*", Poster presentation, 55th Jahrestreffen Deutscher Katalytiker, Weimar, Germany 2022.

National conferences

1. B. Boga, **I. Székely**, K. Hajdu, G. Kovács, Z. Pap, M. Baia, K. Hernádi, L. Nagy, "*The Characterization and the Applicability of Composite Systems Based on WO_3*", Student poster presentation, *Supervisor*, XXIII. International Conference on Chemistry, Deva, Romania, 2017.
2. L.C. Pop, **I. Székely**, M. Rusu, A. Vulpoi, C.I. Fort, L. Baia, C. Coteț, *"Nanoporous Carbons Impregnated with Bi-Fe Nanoparticles and Modified with TiO_2, Study of Their Photocatalytic Activity"*, Poster presentation, XXIII. International Conference on Chemistry, Deva, Romania, 2017.
3. B. Boga, **I. Székely**, R. Csekő, G. Kovács, Z. Pap, M. Baia, K. Hernádi, L. Nagy, "*Photogenerated Electron Transfer in Biological (WO_3/RC) and Inorganic (WO_3/TiO_2) System*", Student poster presentation, *Supervisor*, XXIV. International Conference on Chemistry, Sovata Băi, Romania, 2018.
4. B. Boga, **I. Székely**, T. Szabó, A. M. V. Brânzanic, G. Kovács, Z. Pap, M. Baia, L. Nagy, K. Hernádi, L. Nagy, "*Computational and Experimental Study of RC/WO_3 Based*

Biohybrid System", Student poster presentation, *Supervisor*, XXV. International Conference on Chemistry, Cluj-Napoca, Romania, 2019.

5. B. Boga, **I. Székely**, M. Focșan, Z. Pap, "*The specific case of electron trapping in reaction centre/$WO_3(\cdot 0.33H_2O)$ and $TiO_2/WO_3(\cdot 0.33H_2O)$ systems*", Student poster presentation, *Supervisor*, XXVI. International Conference on Chemistry, Online Conference, Romania, 2020.

References

[1] I. Manisalidis, E. Stavropoulou, A. Stavropoulos, E. Bezirtzoglou, Environmental and Health Impacts of Air Pollution: A Review, Front. Public Heal. 8 (2020) 14. doi:10.3389/fpubh.2020.00014.

[2] L. Lin, H. Yang, X. Xu, Effects of Water Pollution on Human Health and Disease Heterogeneity: A Review, Front. Environ. Sci. 10 (2022). doi:10.3389/fenvs.2022.880246.

[3] R. Fuller, P.J. Landrigan, K. Balakrishnan, G. Bathan, S. Bose-O'Reilly, M. Brauer, J. Caravanos, T. Chiles, A. Cohen, L. Corra, M. Cropper, G. Ferraro, J. Hanna, D. Hanrahan, H. Hu, D. Hunter, G. Janata, R. Kupka, B. Lanphear, M. Lichtveld, K. Martin, A. Mustapha, E. Sanchez-Triana, K. Sandilya, L. Schaefli, J. Shaw, J. Seddon, W. Suk, M.M. Téllez-Rojo, C. Yan, Pollution and health: a progress update, Lancet Planet. Heal. 6 (2022) e535–e547. doi:10.1016/S2542-5196(22)00090-0.

[4] S. Dey, N. Haripavan, S.R. Basha, G.V. Babu, Removal of ammonia and nitrates from contaminated water by using solid waste bio-adsorbents, Curr. Res. Chem. Biol. 1 (2021) 100005. doi:10.1016/j.crchbi.2021.100005.

[5] W.M. Draper, N. Li, G.M. Solomon, Y.C. Heaney, R.B. Crenshaw, R.L. Hinrichs, R.E.P. Chandrasena, Organic Chemical Contaminants in Water System Infrastructure Following Wildfire, ACS Environ. Sci. Technol. Water. 2 (2022) 357–366. doi:10.1021/acsestwater.1c00401.

[6] P. Nowak, K. Kucharska, M. Kamiński, Ecological and health effects of lubricant oils emitted into the environment, Int. J. Environ. Res. Public Health. 16 (2019). doi:10.3390/ijerph16163002.

[7] M. Afzal, K. Rehman, G. Shabir, R. Tahseen, A. Ijaz, A.J. Hashmat, H. Brix, Large-scale remediation of oil-contaminated water using floating treatment wetlands, Npj Clean Water. 2 (2019) 3. doi:10.1038/s41545-018-0025-7.

[8] R. Al-Tohamy, S.S. Ali, F. Li, K.M. Okasha, Y.A.G. Mahmoud, T. Elsamahy, H. Jiao, Y. Fu, J. Sun, A critical review on the treatment of dye-containing wastewater: Ecotoxicological and health concerns of textile dyes and possible remediation approaches for environmental safety, Ecotoxicol. Environ. Saf. 231 (2022) 113160. doi:10.1016/j.ecoenv.2021.113160.

[9] R. Naidu, B. Biswas, I.R. Willett, J. Cribb, B. Kumar Singh, C. Paul Nathanail, F. Coulon, K.T. Semple, K.C. Jones, A. Barclay, R. John Aitken, Chemical pollution: A growing peril and potential catastrophic risk to humanity, Environ. Int. 156 (2021) 106616. doi:10.1016/j.envint.2021.106616.

[10] L.R. Vieira, A.M.V.M. Soares, R. Freitas, Caffeine as a contaminant of concern: A review on concentrations and impacts in marine coastal systems, Chemosphere. 286 (2022) 131675. doi:10.1016/j.chemosphere.2021.131675.

[11] Z. Zhang, Y. Zhou, L. Han, X. Guo, Z. Wu, J. Fang, B. Hou, Y. Cai, J. Jiang, Z. Yang, Impacts of COVID-19 pandemic on the aquatic environment associated with disinfection byproducts and pharmaceuticals, Sci. Total Environ. 811 (2022) 151409.

doi:10.1016/j.scitotenv.2021.151409.
[12] A.L. Srivastav, N. Patel, V.K. Chaudhary, Disinfection by-products in drinking water: Occurrence, toxicity and abatement, Environ. Pollut. 267 (2020) 115474. doi:10.1016/j.envpol.2020.115474.
[13] A.A. Koelmans, N.H. Mohamed Nor, E. Hermsen, M. Kooi, S.M. Mintenig, J. De France, Microplastics in freshwaters and drinking water: Critical review and assessment of data quality, Water Res. 155 (2019) 410–422. doi:10.1016/j.watres.2019.02.054.
[14] M. Syafrudin, R.A. Kristanti, A. Yuniarto, T. Hadibarata, J. Rhee, W.A. Al-Onazi, T.S. Algarni, A.H. Almarri, A.M. Al-Mohaimeed, Pesticides in drinking water-a review, Int. J. Environ. Res. Public Health. 18 (2021) 1–15. doi:10.3390/ijerph18020468.
[15] Bijay-Singh, E. Craswell, Fertilizers and nitrate pollution of surface and ground water: an increasingly pervasive global problem, SN Appl. Sci. 3 (2021) 518. doi:10.1007/s42452-021-04521-8.
[16] S.N. Zulkifli, H.A. Rahim, W.J. Lau, Detection of contaminants in water supply: A review on state-of-the-art monitoring technologies and their applications, Sensors Actuators, B Chem. 255 (2018) 2657–2689. doi:10.1016/j.snb.2017.09.078.
[17] D.A. Gkika, A.C. Mitropoulos, D.A. Lambropoulou, I.K. Kalavrouziotis, G.Z. Kyzas, Cosmetic wastewater treatment technologies: a review, Environ. Sci. Pollut. Res. 29 (2022) 75223–75247. doi:10.1007/s11356-022-23045-1.
[18] C. Benincasa, M. Pellegrino, E. Romano, S. Claps, C. Fallara, E. Perri, Qualitative and Quantitative Analysis of Phenolic Compounds in Spray-Dried Olive Mill Wastewater, Front. Nutr. 8 (2022). doi:10.3389/fnut.2021.782693.
[19] S. Schulze, H. Paschke, T. Meier, M. Muschket, T. Reemtsma, U. Berger, A rapid method for quantification of persistent and mobile organic substances in water using supercritical fluid chromatography coupled to high-resolution mass spectrometry, Anal. Bioanal. Chem. 412 (2020) 4941–4952. doi:10.1007/s00216-020-02722-5.
[20] G. Alberti, C. Zanoni, L.R. Magnaghi, R. Biesuz, Disposable and low-cost colorimetric sensors for environmental analysis, Int. J. Environ. Res. Public Health. 17 (2020) 1–23. doi:10.3390/ijerph17228331.
[21] H. Seok, S. Son, J. Cho, S. Choi, K. Park, C. Kim, N. Jeon, T. Kim, H.U. Kim, Chromism-Integrated Sensors and Devices for Visual Indicators, Sensors. 22 (2022). doi:10.3390/s22114288.
[22] D.C. Aydin, J. Zamudio Pineres, F. Al-Manji, H. Rijnaarts, T. Grotenhuis, Direct analysis of aromatic pollutants using a HPLC-FLD/DAD method for monitoring biodegradation processes, Anal. Methods. 13 (2021) 1635–1642. doi:10.1039/d1ay00083g.
[23] I. Domínguez, F.J. Arrebola, J.L. Martínez Vidal, A. Garrido Frenich, Assessment of wastewater pollution by gas chromatography and high resolution Orbitrap mass spectrometry, J. Chromatogr. A. 1619 (2020) 460964. doi:10.1016/j.chroma.2020.460964.
[24] Q. Liu, Z. Zhao, H. Li, M. Su, S. xuan Liang, Occurrence and removal of organic pollutants by a combined analysis using GC-MS with spectral analysis and acute toxicity, Ecotoxicol.

Environ. Saf. 207 (2021) 111237. doi:10.1016/j.ecoenv.2020.111237.
[25] T. Fernandes, S. Fateixa, M. Ferro, H.I.S. Nogueira, A.L. Daniel-da-Silva, T. Trindade, Colloidal dendritic nanostructures of gold and silver for SERS analysis of water pollutants, J. Mol. Liq. 337 (2021) 116608. doi:10.1016/j.molliq.2021.116608.
[26] M. Saini, S. Augustine, M. Ranjan, T. Som, In-plane optical anisotropy and SERS detection efficiency of self-organized gold nanoparticles on silicon nanoripples: Roles of growth angle and postgrowth annealing, Appl. Surf. Sci. 512 (2020) 145703. doi:10.1016/j.apsusc.2020.145703.
[27] K. Wang, D.W. Sun, H. Pu, Q. Wei, Shell thickness-dependent Au@Ag nanoparticles aggregates for high-performance SERS applications, Talanta. 195 (2019) 506–515. doi:10.1016/j.talanta.2018.11.057.
[28] N. Riswana Barveen, T.J. Wang, Y.H. Chang, In-situ deposition of silver nanoparticles on silver nanoflowers for ultrasensitive and simultaneous SERS detection of organic pollutants, Microchem. J. 159 (2020) 105520. doi:10.1016/j.microc.2020.105520.
[29] P. Butmee, A. Samphao, G. Tumcharern, Reduced graphene oxide on silver nanoparticle layers-decorated titanium dioxide nanotube arrays as SERS-based sensor for glyphosate direct detection in environmental water and soil, J. Hazard. Mater. 437 (2022) 129344. doi:10.1016/j.jhazmat.2022.129344.
[30] D. Singh, R.K. Goswami, K. Agrawal, V. Chaturvedi, P. Verma, Bio-inspired remediation of wastewater: A contemporary approach for environmental clean-up, Curr. Res. Green Sustain. Chem. 5 (2022) 100261. doi:10.1016/j.crgsc.2022.100261.
[31] G.E. Clayton, R.M.S. Thorn, D.M. Reynolds, The efficacy of chlorine-based disinfectants against planktonic and biofilm bacteria for decentralised point-of-use drinking water, Npj Clean Water. 4 (2021) 48. doi:10.1038/s41545-021-00139-w.
[32] A. V. Baskar, N. Bolan, S.A. Hoang, P. Sooriyakumar, M. Kumar, L. Singh, T. Jasemizad, L.P. Padhye, G. Singh, A. Vinu, B. Sarkar, M.B. Kirkham, J. Rinklebe, S. Wang, H. Wang, R. Balasubramanian, K.H.M. Siddique, Recovery, regeneration and sustainable management of spent adsorbents from wastewater treatment streams: A review, Sci. Total Environ. 822 (2022) 153555. doi:10.1016/j.scitotenv.2022.153555.
[33] R. Rashid, I. Shafiq, P. Akhter, M.J. Iqbal, M. Hussain, A state-of-the-art review on wastewater treatment techniques: the effectiveness of adsorption method, Environ. Sci. Pollut. Res. 28 (2021) 9050–9066. doi:10.1007/s11356-021-12395-x.
[34] M. Coha, G. Farinelli, A. Tiraferri, M. Minella, D. Vione, Advanced oxidation processes in the removal of organic substances from produced water: Potential, configurations, and research needs, Chem. Eng. J. 414 (2021) 128668. doi:10.1016/j.cej.2021.128668.
[35] S. Dutta, J. Bhattacharjee, A comparative study between physicochemical and biological methods for effective removal of textile dye from wastewater, in: M.P. Shah, S. Rodriguez-Couto, R.T. Kapoor (Eds.), Dev. Wastewater Treat. Res. Process., Elsevier, 2022: pp. 1–21. doi:10.1016/b978-0-323-85657-7.00003-1.
[36] H. Wang, X. Li, X. Zhao, C. Li, X. Song, P. Zhang, P. Huo, A review on heterogeneous

photocatalysis for environmental remediation: From semiconductors to modification strategies, Chinese J. Catal. 43 (2022) 178–214. doi:10.1016/S1872-2067(21)63910-4.

[37] Y. Gao, N. Yan, C. Jiang, C. Xu, S. Yu, P. Liang, X. Zhang, S. Liang, X. Huang, Filtration-enhanced highly efficient photocatalytic degradation with a novel electrospun rGO@TiO2 nanofibrous membrane: Implication for improving photocatalytic efficiency, Appl. Catal. B Environ. 268 (2020) 118737. doi:10.1016/j.apcatb.2020.118737.

[38] Q. Shang, N. Liu, D. You, Q. Cheng, G. Liao, Z. Pan, The application of Ni and Cu-MOFs as highly efficient catalysts for visible light-driven tetracycline degradation and hydrogen production, J. Mater. Chem. C. 9 (2021) 238–248. doi:10.1039/d0tc04733c.

[39] X. Zhao, P. Wu, Y. Lei, F. Chen, Z. Yu, P. Fang, Y. Liu, Sun-light-driven plasmonic Ag/AgCl@TNT photocatalysts for high-efficient absorption-regeneration and photocatalytic degradation, Appl. Surf. Sci. 529 (2020) 147010. doi:10.1016/j.apsusc.2020.147010.

[40] D. Xiong, W. Zhao, J. Guo, S. Li, Y. Ye, L. E, X. Yang, Highly efficient and reusable BiOCl photocatalyst modulating by hydrogel immobilization and oxygen vacancies engineering, Sep. Purif. Technol. 277 (2021) 119628. doi:10.1016/j.seppur.2021.119628.

[41] A.L. Patterson, The scherrer formula for X-ray particle size determination, Phys. Rev. 56 (1939) 978–982. doi:10.1103/PhysRev.56.978.

[42] P. Kubelka, F. Munk, A contribution to the optics of pigments, Z. Tech. Phys. 12 (1931) 193.

[43] J. Tauc, R. Grigorovici, A. Vancu, Optical Properties and Electronic Structure of Amorphous Germanium, Phys. Status Solidi. 15 (1966) 627–637. doi:https://doi.org/10.1002/pssb.19660150224.

[44] N.F. Mott, E.A. Davis, K. Weiser, Electronic Processes in Non-Crystalline Materials, Phys. Today. 25 (1972) 55–55. doi:10.1063/1.3071145.

[45] T. Menke, Molecular doping of organic semiconductors, 2013. http://www.qucosa.de/fileadmin/data/qucosa/documents/12130/Menke_qucosa.pdf.

[46] I. Székely, E.-Z. Kedves, Z. Pap, M. Baia, Synthesis Design of Electronegativity Dependent WO3 and WO3·0.33H2O Materials for a Better Understanding of TiO2/WO3 Composites' Photocatalytic Activity, Catal. 2021, Vol. 11, Page 779. 11 (2021) 779. doi:10.3390/CATAL11070779.

[47] X. Liu, J. Zhang, T. Yang, X. Guo, S. Wu, S. Wang, Synthesis of Pt nanoparticles functionalized WO3 nanorods and their gas sensing properties, Sensors Actuators, B Chem. 156 (2011) 918–923. doi:10.1016/j.snb.2011.03.006.

[48] B. Boga, I. Székely, Z. Pap, L. Baia, M. Baia, Detailed Spectroscopic and Structural Analysis of TiO2/WO3 Composite Semiconductors, J. Spectrosc. 2018 (2018) 1–7. doi:10.1155/2018/6260458.

[49] I. Székely, M. Baia, K. Magyari, B. Boga, Z. Pap, The effect of the pH adjustment upon the WO3-WO3·0.33H2O-TiO2 ternary composite systems' photocatalytic activity, Appl. Surf. Sci. 490 (2019) 469–480. doi:10.1016/j.apsusc.2019.06.036.

[50] F. Andrei, A. Andrei, R. Birjega, E.N. Sirjita, A.I. Radu, M. Dinescu, V. Ion, V.A. Maraloiu, V.Ş. Teodorescu, N.D. Scarisoreanu, The Influence of the Structural and Morphological Properties of WO3 Thin Films Obtained by PLD on the Photoelectrochemical Water-Splitting Reaction Efficiency, Nanomaterials. 11 (2021) 1–13. doi:10.3390/nano11010110.

[51] S. V. Chong, J.L. Tallon, Aqueous electrochemical insertion of Na+ into the tungsten oxide hybrid WO3(4,4′-bipyridyl)0.5, J. Phys. Chem. Solids. 71 (2010) 303–308. doi:10.1016/j.jpcs.2009.12.081.

[52] B. Boga, I. Székely, M. Focșan, M. Baia, T. Szabó, L. Nagy, Z. Pap, Sensor surface via inspiration from Nature: The specific case of electron trapping in TiO2/WO3(·0.33H2O) and reaction center/WO3(·0.33H2O) systems, Appl. Surf. Sci. 572 (2022) 151139. doi:10.1016/j.apsusc.2021.151139.

[53] I. Székely, Z. Kovács, M. Rusu, T. Gyulavári, M. Todea, M. Focșan, M. Baia, Z. Pap, Tungsten Oxide Morphology-Dependent Au/TiO2/WO3 Heterostructures with Applications in Heterogenous Photocatalysis and Surface-Enhanced Raman Spectroscopy, Catalysts. 13 (2023) 1015. doi:10.3390/catal13061015.

[54] R.E. Darienzo, O. Chen, M. Sullivan, T. Mironava, R. Tannenbaum, Au nanoparticles for SERS: Temperature-controlled nanoparticle morphologies and their Raman enhancing properties, Mater. Chem. Phys. 240 (2020). doi:10.1016/j.matchemphys.2019.122143.